AD-A141 909 A PROGRAM TO IMPROVE SOLARBBLIND UV (ULTRAVIOLET) FLASH LAMPS(U) SCI-TEC INC PRINCETON NJ W J MILLER OCT 83 TR-83-016 N00014-80-C-0763 1/1

UNCLASSIFIED F/G 13/1 NL

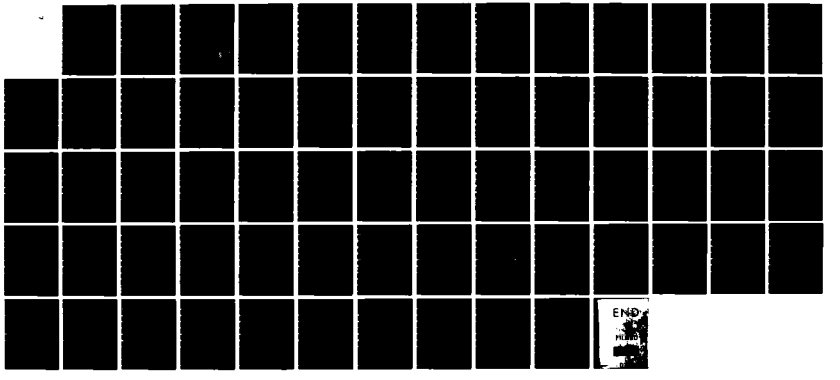

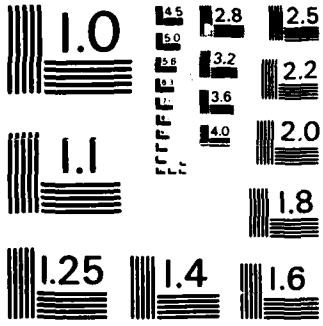

A PROGRAM TO IMPROVE SOLAR BLIND UV FLASH LAMPS

SciTec, Inc.
Princeton New Jersey

SciTec Report No. TR-83-016

A PROGRAM TO IMPROVE SOLAR BLIND UV FLASH LAMPS

Prepared for

OFFICE OF NAVAL RESEARCH
DEPARTMENT OF THE NAVY
800 N. QUINCY ST.
ARLINGTON, VA 22217

October 1983

By

WILLIAM J. MILLER

SCITEC, INC.
P.O. BOX CN 5203
1101 N. STATE ROAD, BLDG. N
PRINCETON, NJ 08540

(609) 921-3892

UNCLASSIFIED

SECURITY CLASSIFICATION OF THIS PAGE (When Data Entered)

REPORT DOCUMENTATION PAGE		READ INSTRUCTIONS BEFORE COMPLETING FORM
1. REPORT NUMBER	2. GOVT ACCESSION NO. AD-A141 909	3. RECIPIENT'S CATALOG NUMBER
4. TITLE (and Subtitle) A Program to Improve Solar Blind UV Flash Lamps		5. TYPE OF REPORT & PERIOD COVERED 1 Sep 80 - 31 May 82
		6. PERFORMING ORG. REPORT NUMBER TR-83-016
7. AUTHOR(s) William J. Miller		8. CONTRACT OR GRANT NUMBER(s) N00014-80-C-0763
9. PERFORMING ORGANIZATION NAME AND ADDRESS SciTec, Inc. P.O. Box CN 5203 Princeton, NJ 08540		10. PROGRAM ELEMENT, PROJECT, TASK AREA & WORK UNIT NUMBERS
11. CONTROLLING OFFICE NAME AND ADDRESS Office of Naval Research Department of the Navy 800 N. Quincy St., Arlington, VA 22217		12. REPORT DATE October 1983
		13. NUMBER OF PAGES 56
14. MONITORING AGENCY NAME & ADDRESS(if different from Controlling Office) Same		15. SECURITY CLASS. (of this report) Unclassified
		15a. DECLASSIFICATION/DOWNGRADING SCHEDULE N/A

16. DISTRIBUTION STATEMENT (of this Report)

Approved for public release; distribution unlimited.

17. DISTRIBUTION STATEMENT (of the abstract entered in Block 20, if different from Report)

Same

18. SUPPLEMENTARY NOTES

Dr. Van O. Nicolai, Contract Monitor

19. KEY WORDS (Continue on reverse side if necessary and identify by block number)

Ultraviolet Lamps
Light Sources
Xenon Lamps
Solar Blind UV

20. ABSTRACT (Continue on reverse side if necessary and identify by block number)

A study was conducted of UV light sources, particularly Xenon/H_2 flash lamps, in an effort to achieve higher efficiencies in the upper end of the solar blind wavelength region for application to UV communication devices. Lamps containing a number of inert gases, with and without added H_2, were subjected to detailed spectroscopic examination and their UV output efficiencies compared to that of conventional commercially available lamps of

DD FORM 1 JAN 73 1473 EDITION OF 1 NOV 65 IS OBSOLETE

UNCLASSIFIED

SECURITY CLASSIFICATION OF THIS PAGE (When Data Entered)

similar physical configuration. A highly versatile power supply capable of delivering very short pulses at variable frequency and power level was designed and built for this purpose. It incorporates the capability to hold off capacitor recharge for specifiable times between pulses in order to minimize premature lamp firing which produces holdover and renders the source useless for FM or pulse position modulation operation. Modest increases in efficiency were achieved by increasing Xe pressure and operating the lamps at the highest power and voltage levels compatible with the structural strength of the lamp and the frequency range selected for operation. Xe/H_2 continue to be judged the optimum fill gas in preference to He, Ne, or Ar mixtures. The maximum attainable efficiency, defined as light output in the 260-280 nm range divided by the total electrical power to the lamp electrodes, appears to be about 0.4% achievable over a fairly broad range of electrical operating parameters, H_2 partial pressure and arc gap.

TABLE OF CONTENTS

LIST OF FIGURES

LIST OF FIGURES (Continued)

LIST OF TABLES

1. INTRODUCTION

The requirement for more intense and efficient ultraviolet light sources has received considerable impetus in recent years for several reasons, including the development of an ultraviolet (UV) communications system (Ref. 1). State-of-the-art UV lamps presently available are used primarily in spectroscopic applications, either for wavelength calibration, as sources for absorption spectrophotometry or as solar simulators. Technically, these light sources appear to have changed very little in decades. Contemporary requirements for such lamps include the ability to perform in a pulsed mode with controllable pulse duration, reproducible high intensity characteristics, long life and greater efficiency particularly in the solar blind region with as little interference from visible IR and near UV radiation as possible. The applications envisioned for these light sources often require a high degree of portability thus prohibiting the use of large bulky power supplies such as those typically used to operate high pressure arc lamps and thereby creating the need for high power efficiency. High pressure arc lamps, because of their inherent high temperature characteristics, also produce large quantities of visible, near UV and IR radiation which, in these applications, have to be reduced or eliminated by selective filtering. The simultaneous attainment of satisfactory rejection of high intensity sideband radiation and the adequate transmission of UV puts severe practical demands on light filters which can result in thermal stability problems and low output light levels. Substantial improvements in the performance and efficiency of UV flash lamps would therefore make it unnecessary to pursue other possibly more difficult problems.

Low and intermediate (0.01 - 5 atm) pressure electrical discharge lamps are the most efficient UV sources currently available and appear to be the ones best suited to communications applications. Their performance

however is a limiting factor in the development of more effective UV communication systems. The objective of this program was the improvement of the UV output efficiency and performance characteristics of these flashlamps. The pursuit of this objective involved two different approaches. The first consisted of a detailed quantitative investigation of the performance and emission characteristics of existing state-of-the-art lamps and extensive documentation of the effects of changes in their operating parameters. Secondly, an attempt was made to formulate novel gas mixtures and electronic techniques which would provide more light in the spectral regions of prime interest without sacrificing overall lamp efficiency and without compromising other requisite lamp characteristics such as size, portability, pulse frequency and duration and lamp life. The first objective was met. Tentative conclusions based on preliminary experiments utilizing isolated lamp samples were verified and lamp performance characteristics were determined using a wide variety of gas mixtures, fill pressures, arc gaps and excitation pulse configurations. Modest increases in lamp efficiency were attained and data establishing probable limitations on the further extension of such improvement were obtained. None of the more novel attempts to achieve higher efficiency were successful.

2. BACKGROUND

2.1 UV Lamps

The three discharge lamps most commonly employed as UV light sources are filled with Hg, Xe or D_2. The emission characteristics of these low pressure lamps under their typical recommended operating conditions are given in Figure 1. It can be seen that in the wavelength region between 200 - 300 nm, the Hg "pen lamp" is by far the strongest emitter. This emission, however, arises from an atomic resonance transition and the resultant narrow line comprises the only significant radiation throughout the entire solar blind portion of the UV. The width of this line is on the order of 0.10 nm. Typical Xe lamp emission, under ordinary operating conditions with about 5-10 watts input power yields about 0.02 watts of output (Ref. 2) over the entire 200 - 300 nm bandpass compared to about 0.3 watts for the low pressure Hg lamp which consumes slightly less power. The D_2 discharge lamp intensity is considerably lower than either of the latter two. This type of lamp has, however, become the calibration reference standard (Ref. 3) for UV sources largely because of its remarkable reproducibility and stability.

The spectral distributions of emissions from these lamps are not only functions of the gas pressure within the lamp, but also functions of the electrical characteristics of the discharge. Figure 2 (from Ref. 2) shows the spectral output from a high pressure Xe arc lamp powered by 50 joules/second at two different voltages (Ref. 4). High voltages appear to produce more UV radiation at the expense of emission in the visible and IR. As a first approximation, the limitations on the amount of light that can be obtained in the UV can be considered to be imposed by the physical strength of the bulb envelope, and by the decay characteristics of the light output pulse with time. For the same amount of input electrical power,

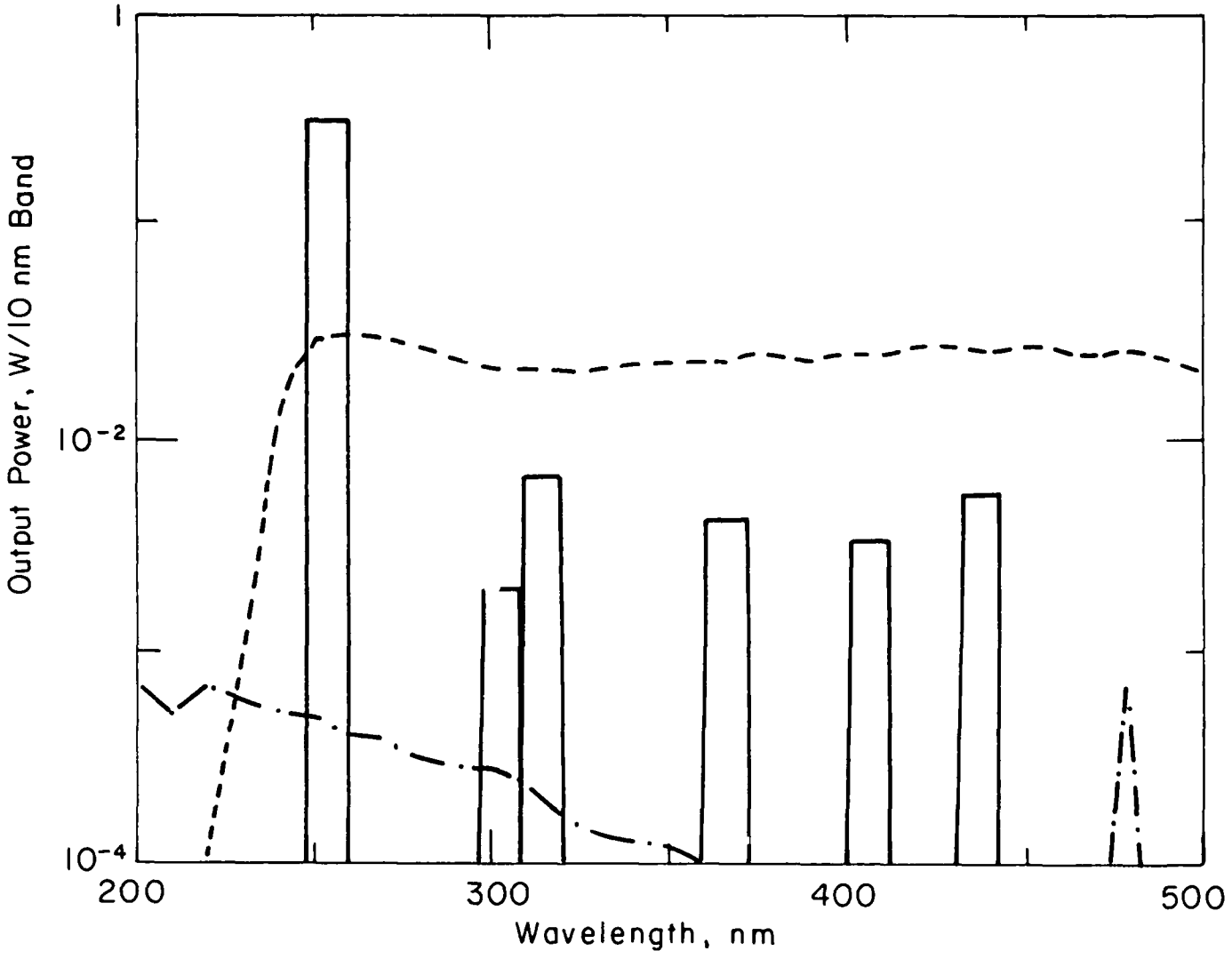

Figure 1. Comparative Output Power for 3 UV Lamps for 10 nm Bandwidths
—— low pressure Hg --- Xe -·- D_2

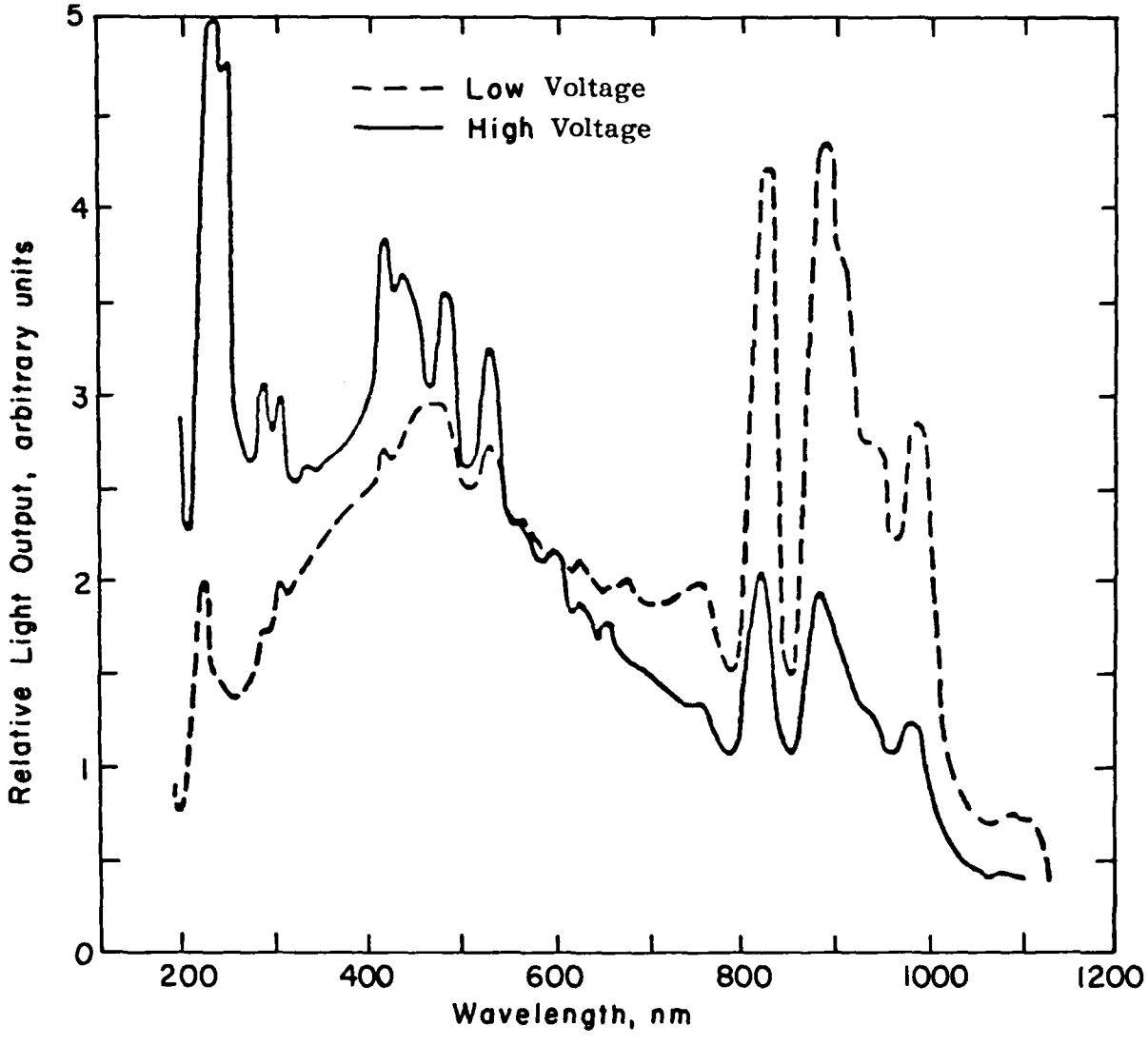

Figure 2. Effect of Discharge Voltage on Xe Arc Lamp Spectrum

shorter pulses decrease bu. life. Conversely at any fixed value of pulse duration, increased input power decreases bulb life. The approximate relationship between input power, I, and pulse duration, t, for constant bulb life and given bulb size is $I = at^2$. The root cause of these limitations is heat. If cooling can be provided or if the quartz envelope can be moved away from the discharge, more power and/or longer pulses can be tolerated without adversely decreasing bulb life or output.

The efficiencies of the various UV light sources currently available vary at least as greatly as do their spectral energy distributions. Efficiency figures for the sources of Figure 1 are given in Figure 3. These values were obtained by simply dividing the power output exhibited in Figure 1 by the electrical power input to just the lamp (not the entire device) in each case. The extreme efficiency of the low pressure Hg lamp is immediately apparent. More than 90% of the radiation is in the 254 nm line and, overall, about 10% of the input energy is converted to light at this wavelength. The seemingly attractive features of the Hg lamp in terms of both preferential output and conversion efficiency are unfortunately offset by other undesirable factors. First, the fact that the emitting species is initially a liquid with a low nonoptimum vapor pressure means that a warm up period is required, and that the intensity is somehow dependent on the lamp temperature which changes continuously during the period of operation. Secondly, the lifetime of the excited state (Ref. 5) and the absorption cross sections for the Hg ground state produce a pulse of long duration which limits the frequency of device operation. Despite the fact that the Hg 254 nm line is due to a "forbidden" $^3P_1 \rightarrow {}^1S_0$ transition, it has a radiative lifetime of about 3 nsec - a value much more characteristic of a fully allowed transition than one involving a change of multiplicity. The large emission and absorption coefficients corresponding to this short lifetime, coupled with the fact that the lower level of the transition is the atomic ground state of the atom dictate that light will be absorbed and

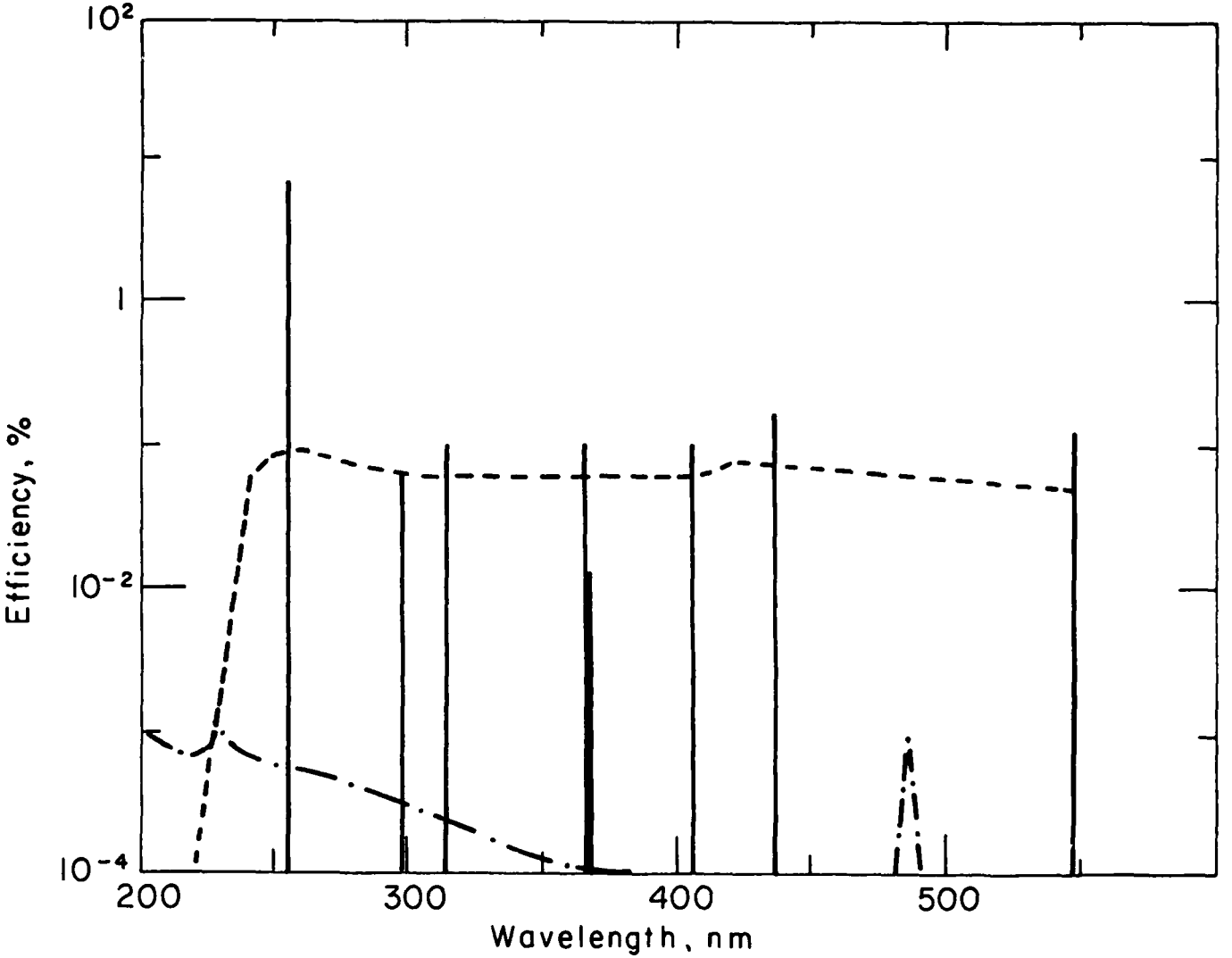

Figure 3. Comparative Light Output Efficiencies for Lamps of Figure 1

reemitted many times in even the low pressure Hg atmosphere of these lamps before it reaches and passes through the walls of the quartz vessel. Measurements on Hg pen lamps fabricated from only 1 mm bore quartz tubing indicate that a typical practically obtainable pulse width (half-maximum) is about 52 microseconds (Ref. 6). Such a pulse width is unacceptably long for FM devices. Finally, and most importantly, it will be seen that 254 nm does not lie within the optimum spectral region with respect to atmospheric transmission.

The standard D_2 lamp contains a very small discharge. Its light emanates from an aperture which is typically only 1-2 mm in diameter. The glow itself within the quartz tube envelope is a few mm long and about 1 mm in diameter. Most of the continuum emission is due to the $a^3\,\Sigma^+_g \quad b^3\,\Sigma^+_u$ transition (Ref. 7), the lower state of which is repulsive. Higher current densities or gas pressures in H_2 or D_2 lamps lead to greater degrees of molecular dissociation and to displacement of the most intense emission to wavelengths both above and below the desired solar blind region. Atomic hydrogen or D has no lines of any significance in the bandpass of interest and its presence is therefore of no radiative advantage, whatsoever, in a UV lamp. In fact, its very high diffusion coefficient and reactivity are sources of potential problems with envelope integrity and electrode metallurgy. High power versions of D_2 lamps are therefore unlikely to serve the purposes of a UV lamp very well.

It is clear from the foregoing considerations why Xe lamps were chosen for the UV communication system. In the case of the Xe discharge lamp used in the transmitter described in Ref. 1, a small amount of H_2 is added to the lamp gas fill not for its contribution to the emission but to increase the rate of pulse decay, shorten the pulse width and prevent the discharge from holding over and becoming continuous with respect to time. The H_2 may produce this effect by enhancing the rate of removal of current-conducting charged species created during the pulse. This may occur

through an increase in the rate of recombination via the formation of negative ions which have much larger neutralization cross sections than do electrons in collisions with positive atomic ions. Alternatively, the H_2 may act by quenching easily ionizable Xe metastable states via electronic/vibrational energy transfer. In general, processes such as the latter are too slow to be of significance but the multitude of energy levels associated with many electron atoms and ions such as Xe, Xe^+ and Xe^{++} greatly enhances the probability of occurrence of exact resonances at which energy transfer is extremely efficient.

A recent study (Ref. 8) of means to improve UV communication system components sponsored by NOSC revealed that some improvement in UV output efficiency could be obtained by increasing the Xe pressure within the lamp and that the lamp performance was only slightly sensitive to H_2 partial pressure or electrode spacing. The study involved the use of 5 specially designed lamps, two of which were nominally state-of-the-art conventional design, one with reduced H_2 content, another with a 50% larger gap than normal between the electrodes and the fifth with two times the normal fill pressure of Xe. The results are presented in Table 1. It can be seen that only the higher pressure lamp performed more efficiently than the two conventional ones and that the improvement achieved is on the same order as that of the differences between the nominally identical lamps 1 and 2. The limited number of devices employed in this study made it impossible to establish trends from this information, but at least one positive indication in terms of improved performance was obtained.

2.2 Pertinent Spectral Reference Data

Since line emission is an extremely important component of the radiation from both Xe and Hg discharges, it seemed appropriate to give consideration to the comparative abundances of the spectral lines of each of the inert gas atoms and ions. The lamp fill gases of principal interest in

	Input Power, Watts	Output UV, Milliwatts	Efficiency %
Standard "Old" #1	25.6	51.3	0.20
Standard "New" #1	25.9	69.9	0.27
Standard "New" #2	24.3	63.3	0.26
Low H_2 Design	25.6	64.0	0.25
Large Arc Gap	25.7	54.0	0.21
High Xe Pressure	25.2	78.0	0.31

Table 1. Total Radiant Power and Lamp Efficiencies in Solar Blind for Various Xe/H_2 Lamps (Ref. 8)

this study were the inert gases He, Ne, Ar, Xe and H_2 and Hg. The principal spectral lines for each of the elements involved and their important ions are summarized in Tables 2 through 6. All of the inert gas data was taken from Ref. 9; the Hg line intensities are from a Handbook (Ref. 10).

Interestingly, neutral Xe has no strong lines in the spectral region of interest; all of the significant line radiation observed is attributable to Xe^+ and Xe^{++}. On this basis, then, Ar, which also displays no atomic line emission but which does have a multitude of Ar^+ ionic lines, could not be eliminated as a candidate fill gas. Continuing this line of evaluation, one would be led to conclude that He would be an unlikely emitter and that Ne would hold great promise by virtue of the abundance of lines in the spectra of both neutrals and ions. It will be seen in the description of results to follow that none of these generalizations proved valid and that a priori rationalizations of this nature were, in the end, useless.

2.3 Atmospheric Transmission Considerations

As noted by Neer and Schlupf in Ref. 8, total solar blindness is not a stringent requirement even in UV communication systems where background radiation can be an important problem. Variations in received signal intensity induced by changes in absorption due to atmospheric O_3 is a far more significant consideration. The effects of absorption and molecular scattering combined with the properties of solar blind filter materials led these workers to the conclusion that optimum spectral region for these purposes is 270 - 280 nm. The atmospheric transmission data presented in Figures 4 and 5 illustrate the most important of these effects. At realistic atmospheric O_3 concentrations, the region below 280 nm can be seen to become virtually opaque at distances greater than a few kilometers. As the practical ramifications of these absorption and scattering effects became evident during the course of our experimental program, attention was quite

Hg I

λ, A	I	E_u, eV	E_g, eV	Transition	J
2967.28	100	4.67	8.85	$6d^3D—6p^3P°$	0-1
2893.60	40	4.89	9.17	$8s^3S—6p^3P°$	1-1
2752.78	140	4.67	9.17	$8s^3S—6p^3P°$	1-0
2536.52	2000	0	4.89	$6p^3P°—6s^21s$	1-0

Table 2. Principal Emission Lines for Mercury in the Wavelength Interval 2500-3000A (Ref. 10)

He I

λ, A	I	E_u, eV	E_g, eV	Transition	J
2945,106	100	19,82	24,03	$2s\ ^3S—5p\ ^3P°$	1—2, 1, 0
2829,076	40	19,82	24,20	$2s\ ^3S—6p\ ^3P°$	1—2, 1, 0
2763,804	20	19,82	24,30	$2s\ ^3S—7p\ ^3P°$	1—2, 1, 0
2723,191	10	19,82	24,37	$2s\ ^3S—8p\ ^3P°$	1—2, 1, 0
2696,119	7	19,82	24,42	$2s\ ^3S—9p\ ^3P°$	1—2, 1, 0
2677,135	5	19,82	24,45	$2s\ ^3S—10p\ ^3P°$	1—2, 1, 0
2663,271	4	19,82	24,47	$2s\ ^3S—11p\ ^3P°$	1—2, 1, 0
2652,848	3	19,82	24,49	$2s\ ^3S—12p\ ^3P°$	1—2, 1, 0
2644,802	2	19,82	24,50	$2s\ ^3S—13p\ ^3P°$	1—2, 1, 0
He II,					
2733,32	100	48,37	52,90	$3d\ ^3D—6f\ ^3F°$ etc.	$^5/_2$, $^3/_2—^7/_2$, $^5/_2$
2511,22	50	48,37	53,30	$3d\ ^3D—7f\ ^3F°$ etc.	

Table 3. Principal Emission Lines for Neutral and Ionized Helium in the Wavelength Interval 2500-3000A (Ref. 9)

λ, Å	I	E_H, eV	E_B, eV	Transition	J
2994,250	3	16,67	20,81	$3s\ [1^1/_2]°—4f'\ [2^1/_2]$	1—2
2992,438	200	16,62	20,76	$3s\ [1^1/_2]°—5p\ [1/_2]$	2—1
2992,420	200	16,67	20,81	$3s\ [1^1/_2]°—5p\ [1/_2]$	1—0
2982,663	300	16,62	20,77	$3s\ [1^1/_2]°—5p\ [2^1/_2]$	2—3
2980,922	50	16,71	20,87	$3s'\ [1/_2]°—5p'\ [1^1/_2]$	0—1
2980,642	40	16,71	20,87	$3s'\ [1/_2]°—5p'\ [1/_2]$	0—1
2979,806	50	16,62	20,78	$3s\ [1^1/_2]°—5p\ [2^1/_2]$	2—2
2975,518	35	16,62	20,78	$3s\ [1^1/_2]°—5p\ [1^1/_2]$	2—1
2974,714	300	16,62	20,78	$3s\ [1^1/_2]°—5p\ [1^1/_2]$	2—2
2957,293	8	16,62	20,81	$3s\ [1^1/_2]°—4f'\ [2^1/_2]$	2—2, 3
2952,527	5	16,85	21,05	$3s'\ [1/_2]°—5p\ [1/_2]$	1—1
2949,316	15	16,67	20,87	$3s\ [1^1/_2]°—5p'\ [1^1/_2]$	1—1
2949,043	10	16,67	20,87	$3s\ [1^1/_2]°—5p'\ [1/_2]$	1—1
2947,297	200	16,67	20,88	$3s\ [1^1/_2]°—5p'\ [1^1/_2]$	1—2
2946,732	2	16,85	21,05	$3s'\ [1/_2]°—6p\ [2^1/_2]$	1—2
2944,575	2	16,85	21,06	$3s'\ [1/_2]°—6p\ [1^1/_2]$	1—1
2932,721	100	16,85	21,07	$3s'\ [1/_2]°—6p\ [1/_2]$	1—0
2929,312	15	16,67	20,90	$3s\ [1^1/_2]°—5p'\ [1/_2]$	1—0
2913,417	2	16,62	20,87	$3s\ [1^1/_2]°—5p'\ [1^1/_2]$	2—1
2913,168	200	16,62	20,87	$3s\ [1^1/_2]°—5p'\ [1/_2]$	2—1
2911,461	25	16,62	20,88	$3s\ [1^1/_2]°—5p'\ [1/_2]$	2—2
2881,852	2	16,85	21,15	$3s'\ [1/_2]°—6p'\ [1/_2]$	1—1
2880,290	3	16,85	21,15	$3s'\ [1/_2]°—6p'\ [1^1/_2]$	1—2
2872,663	35	16,85	21,16	$3s'\ [1/_2]°—6p'\ [1/_2]$	1—0
2862,070	8	16,71	21,05	$3s'\ [1/_2]°—6p\ [1/_2]$	0—1
2846,490	2	16,85	21,20	$3s'\ [1/_2]°—7p\ [1/_2]$	1—1
2842,632	15	16,85	21,21	$3s'\ [1/_2]°—7p\ [1^1/_2]$	1—1
2835,233	15	16,85	21,22	$3s'\ [1/_2]°—7p\ [1/_2]$	1—0
2832,921	8	16,67	21,05	$3s\ [1^1/_2]°—6p\ [1/_2]$	1—1
2827,584	3	16,67	21,05	$3s\ [1^1/_2]°—6p\ [2^1/_2]$	1—2
2825,609	8	16,67	21,06	$3s\ [1^1/_2]°—6p\ [1^1/_2]$	1—1
2825,259	10	16,67	21,06	$3s\ [1^1/_2]°—6p\ [1^1/_2]$	1—2
2814,685	20	16,67	21,07	$3s\ [1^1/_2]°—6p\ [1/_2]$	1—0
2799,80	2	16,62	21,05	$3s\ [1^1/_2]°—6p\ [1/_2]$	2—1
2795,963	8	16,62	21,07	$3s\ [1^1/_2]°—6p\ [2^1/_2]$	2—3
2795,613	1	16,71	21,15	$3s'\ [1/_2]°—6p'\ [1/_2]$	0—1
2795,101	35	16,71	21,15	$3s'\ [1/_2]°—6p\ [1^1/_2]$	0—1
2794,592	5	16,62	21,05	$3s\ [1^1/_2]°—6p\ [2^1/_2]$	2—2
2792,660	3	16,62	21,06	$3s\ [1^1/_2]°—6p\ [1^1/_2]$	2—1
2792,318	20	16,62	21,06	$3s\ [1^1/_2]°—6p\ [1^1/_2]$	2—2
2782,07	2	16,85	21,30	$3s'\ [1/_2]°—7p'\ [1^1/_2]$	1—1
2781,68	3	16,85	21,30	$3s'\ [1/_2]°—7p'\ [1^1/_2]$	1—2
2775,049	5	16,85	21,31	$3s'\ [1/_2]°—7p'\ [1^1/_2]$	1—0
2767,77	2	16,67	21,15	$3s\ [1^1/_2]°—6p'\ [1/_2]$	1—1
2767,28	3	16,67	21,15	$3s\ [1^1/_2]°—6p'\ [1^1/_2]$	1—1
2766,364	3	16,67	21,15	$3s\ [1^1/_2]°—6p'\ [1^1/_2]$	1—2
2762,324	3	16,71	21,20	$3s'\ [1/_2]°—7p\ [1^1/_2]$	0—1
2759,323	2	16,67	21,16	$3s\ [1^1/_2]°—6p'\ [1/_2]$	1—0
2758,64	3	16,71	21,21	$3s'\ [1/_2]°—7p\ [1^1/_2]$	0—1
2755,82	15	16,62	21,12	$3s\ [1^1/_2]°—5f'\ [2^1/_2]$	2—2, 3
2743,53	15	16,85	21,36	$3s'\ [1/_2]°—9p\ [1/_2]$	1—0
2736,177	5	16,62	21,15	$3s\ [1^1/_2]°—6p'\ [1/_2]$	2—1
2735,69	8	16,62	21,15	$3s\ [1^1/_2]°—6p'\ [1^1/_2]$	2—1
2735,168	3	16,67	21,20	$3s\ [1^1/_2]°—7p\ [1^1/_2]$	1—1
2734,755	2	16,62	21,15	$3s\ [1^1/_2]°—6p'\ [1^1/_2]$	2—2
2732,61	1	16,67	21,21	$3s\ [1^1/_2]°—7p\ [2^1/_2]$	1—2
2731,528	3	16,67	21,21	$3s\ [1^1/_2]°—7p\ [1^1/_2]$	1—1
2731,358	3	16,67	21,21	$3s\ [1^1/_2]°—7p\ [1^1/_2]$	1—2
2724,772	3	16,67	21,22	$3s\ [1^1/_2]°—7p\ [1/_2]$	1—0
2704,32	2	16,62	21,20	$3s\ [1^1/_2]°—7p\ [1/_2]$	2—1
2702,554	3	16,62	21,20	$3s\ [1^1/_2]°—7p\ [2^1/_2]$	2—3
2701,766	2	16,62	21,21	$3s\ [1^1/_2]°—7p\ [2^1/_2]$	2—2
2701,653	2	16,71	21,30	$3s'\ [1/_2]°—7p'\ [1^1/_2]$	0—1
2700,681	2	16,62	21,21	$3s\ [1^1/_2]°—7p\ [1^1/_2]$	2—1
2700,555	8	16,62	21,21	$3s\ [1^1/_2]°—7p\ [1^1/_2]$	2—2
2680,685	1	16,85	21,46	$3s'\ [1/_2]°—9p\ [1/_2]$	1—0
2679,19	2	16,67	21,29	$3s\ [1^1/_2]°—8p\ [1/_2]$	1—1
2677,87	2	16,67	21,30	$3s\ [1^1/_2]°—8p\ [2^1/_2]$	1—2
2677,020	1	16,67	21,30	$3s\ [1^1/_2]°—8p\ [1^1/_2]$	1—1
2675,64	200	16,67	21,30	$3s\ [1^1/_2]°—7p'\ [1^1/_2]$	1—1
2675,24	200	16,67	21,30	$3s\ [1^1/_2]°—7p'\ [1^1/_2]$	1—2
2669,13	3	16,67	21,30	$3s\ [1^1/_2]°—8p\ [1/_2]$	1—0
		16,67	21,31	$3s\ [1^1/_2]°—7p'\ [1/_2]$	1—0
2657,52	15	16,85	21,51	$3s'\ [1/_2]°—10p'\ [1/_2]$	1—0
2648,56	25	16,62	21,30	$3s\ [1^1/_2]°—8p\ [2^1/_2]$	2—3
2648,21	15	16,62	21,30	$3s\ [1^1/_2]°—8p\ [2^1/_2]$	2—2
2647,76	8	16,71	21,39	$3s'\ [1/_2]°—8p'\ [1^1/_2]$	0—1
2647,42	200	16,62	21,30	$3s\ [1^1/_2]°—8p\ [1^1/_2]$	2—2, 1
2646,19	15	16,62	21,30	$3s\ [1^1/_2]°—7p'\ [1^1/_2]$	2—1
2645,645	35	16,62	21,30	$3s\ [1^1/_2]°—7p'\ [1^1/_2]$	2—2
2644,16	5	16,85	21,53	$3s'\ [1/_2]°—11p'\ [1/_2]$	1—0
2642,47	8	16,67	21,36	$3s\ [1^1/_2]°—9p\ [1^1/_2]$	1—2, 1
2639,97	15	16,67	21,36	$3s\ [1^1/_2]°—9p\ [1/_2]$	1—0
2636,070	25	16,85	21,55	$3s'\ [1/_2]°—12p'\ [1/_2]$	1—0
2622,90	15	16,67	21,40	$3s\ [1^1/_2]°—8p'\ [1^1/_2]$	1—2, 1
2616,62	25	16,67	21,40	$3s\ [1^1/_2]°—8p'\ [1^1/_2]$	1—0
2614,26	5	16,62	21,36	$3s\ [1^1/_2]°—9p\ [2^1/_2]$	2—3
2613,94	2	16,62	21,36	$3s\ [1^1/_2]°—9p\ [2^1/_2]$	2—2
2613,59	30	16,62	21,36	$3s\ [1^1/_2]°—9p\ [1^1/_2]$	2—2, 1

Table 4. Principal Emission Lines for Neutral and Ionized Neon in the Wavelength Interval 2600-3000A (Ref. 9)

Ne II

λ, Å	I	E_H, eV	E_B, eV	Transition	J
2973,07	1	34,02	38,18	$3p'\ ^2F°—3d'\ ^2F$	$^5/_2—^7/_2$
2967,181	3	34,02	38,20	$3p'\ ^2F°—3d'\ ^2F$	$^7/_2—^5/_2$
2963,235	2	34,02	38,20	$3p'\ ^2F°—3d'\ ^2F$	$^5/_2—^5/_2$
2955,73	7	27,17	31,36	$3s\ ^4P—3p\ ^4S°$	$^5/_2—^3/_2$
2953,10	0	30,55	34,75	$3p\ ^4P°—3d\ ^2D$	$^3/_2—^5/_2$
2951,10	2	30,57	34,77	$3p\ ^4P°—3d\ ^2D$	$^1/_2—^3/_2$
2935,30	1	30,55	34,77	$3p\ ^4P°—3d\ ^2D$	$^3/_2—^3/_2$
2933,70	2	30,52	34,75	$3p\ ^4P°—3d\ ^2D$	$^5/_2—^5/_2$
2925,623	3	30,57	34,81	$3p\ ^4P°—3d\ ^4P$	$^1/_2—^1/_2$
2916,16	1	30,52	34,77	$3p\ ^4P°—3d\ ^2D$	$^5/_2—^3/_2$
2910,059	5	30,55	34,81	$3p\ ^4P°—3d\ ^4P$	$^3/_2—^1/_2$
2906,815	3	30,57	34,84	$3p\ ^4P°—3d\ ^4P$	$^1/_2—^3/_2$
2897,03	2	30,52	34,80	$3p\ ^4P°—3d\ ^4F$	$^5/_2—^7/_2$
2891,36	0,5	30,55	34,84	$3p\ ^4P°—3d\ ^4P$	$^3/_2—^3/_2$
2888,43	1	30,55	34,84	$3p\ ^4P°—3d\ ^4F$	$^3/_2—^5/_2$
2878,13	0,5	30,57	34,88	$3p\ ^4P°—3d\ ^2P$	$^1/_2—^1/_2$
2876,43	4	30,52	34,83	$3p\ ^4P°—3d\ ^4F$	$^5/_2—^3/_2$
2873,00	3	30,52	34,84	$3p\ ^4P°—3d\ ^4P$	$^5/_2—^3/_2$
2869,95	2	30,52	34,84	$3p\ ^4P°—3d\ ^4F$	$^5/_2—^5/_2$
2858,01	2	30,52	34,86	$3p\ ^4P°—3d\ ^4P$	$^5/_2—^5/_2$
2809,50	4	30,55	34,96	$3p\ ^4P°—4s\ ^4P$	$^3/_2—^5/_2$
2794,220	3	30,57	35,01	$3p\ ^4P°—4s\ ^4P$	$^1/_2—^3/_2$
2792,015	5	30,52	34,96	$3p\ ^4P°—4s\ ^4P$	$^5/_2—^5/_2$
2780,023	2	30,55	35,01	$3p\ ^4P°—4s\ ^4P$	$^3/_2—^3/_2$
2770,06	1	30,57	35,05	$3p\ ^4P°—4s\ ^4P$	$^1/_2—^1/_2$
2762,922	3	30,52	35,01	$3p\ ^4P°—4s\ ^4P$	$^5/_2—^3/_2$
2756,716	3	30,55	35,05	$3p\ ^4P°—4s\ ^4P$	$^3/_2—^1/_2$

Ne III

λ, Å	I	E_H, eV	E_B, eV	Transition	J
2825,82	5	46,43	50,81	$3s''\ ^3P°—3p''\ ^3D$	0—1
2825,28	4	46,42	50,81	$3s''\ ^3P°—3p''\ ^3D$	1—2
2824,47	3	46,42	50,82	$3s''\ ^3P°—3p''\ ^3D$	1—1
2822,95	7	46,42	50,81	$3s''\ ^3P°—3p''\ ^3D$	2—3
2802,34	2	46,42	50,85	$3s''\ ^3P°—3p''\ ^3S$	1—1
2800,24	3	46,42	50,85	$3s''\ ^3P°—3p''\ ^3S$	2—1
2787,73	4	43,79	48,23	$3s'\ ^3D°—3p'\ ^3D$	1—1
2786,89	3	43,79	48,23	$3s'\ ^3D°—3p'\ ^3D$	1—2
2786,17	2	43,79	48,23	$3s'\ ^3D°—3p'\ ^3D$	2—1
2785,29	5	43,79	48,23	$3s'\ ^3D°—3p'\ ^3D$	2—2
2783,03	2	43,78	48,24	$3s'\ ^3D°—3p'\ ^3D$	3—2
2777,65	7	43,78	48,24	$3s'\ ^3D°—3p'\ ^3D$	3—3
2678,64	25	39,60	44,23	$3s\ ^3S°—3p\ ^3P$	1—1
2677,90	30	39,60	44,23	$3s\ ^3S°—3p\ ^3P$	1—2, 0
2642,42	3	46,42	51,12	$3s''\ ^3P°—3p''\ ^3P$	1—0
2642,25	2	46,42	51,12	$3s''\ ^3P°—3p''\ ^3P$	0—1
2641,07	10	46,42	51,12	$3s''\ ^3P°—3p''\ ^3P$	1—1
2640,56	6	46,42	51,12	$3s''\ ^3P°—3p''\ ^3P$	1—2
2639,18	5	46,42	51,12	$3s''\ ^3P°—3p''\ ^3P$	2—1
2638,70	10	46,42	51,12	$3s''\ ^3P°—3p''\ ^3P$	2—2
2615,87	10	43,79	48,53	$3s'\ ^3D°—3p'\ ^3F$	1—2
2614,51	4	43,79	48,53	$3s'\ ^3D°—3p'\ ^3F$	2—2
2613,41	12	43,79	48,53	$3s'\ ^3D°—3p'\ ^3F$	2—3
2611,42	4	43,78	48,53	$3s'\ ^3D°—3p'\ ^3F$	3—3
2610,03	15	43,78	48,53	$3s'\ ^3D°—3p'\ ^3F$	3—4
2595,68	20	38,95	43,72	$3s\ ^5S°—3p\ ^5P$	2—1
2593,60	30	38,95	43,72	$3s\ ^5S°—3p\ ^5P$	2—2
2590,04	40	38,95	47,73	$3s\ ^5S°—3p\ ^5P$	2—3

Table 4. Principal Emission Lines for Neutral and Ionized Neon in the Wavelength Interval 2600-3000A (Ref. 9)(Continued)

Ar II

λ, Å	I	E_H, eV	E_B, eV	Transition	J
2999,110	2	20,24	24,38	$3d'\ ^2F—(^3P_0)\ 4f\ [3]^c$	$^5/_2—^5/_2$
2990,843	2	21,43	25,57	$3d'\ ^2D—(^3P_1)\ 5f\ [3]^\circ$	$^3/_2—^5/_2$
2979,051	15	17,26	21,43	$4s\ ^2P—4p'\ ^2P^\circ$	$^1/_2—^1/_2$
2960,260	5	21,67	25,86	$3d'\ ^2P—(^1D)\ 4f\ [1]^c$	$^1/_2—^1/_2$
		21,67	25,86	$3d'\ ^2P—(^1D)\ 4f\ [1]^\circ$	$^1/_2—^3/_2$
2957,532	3	21,43	25,62	$3d'\ ^2D—(^3P_0)\ 5f\ [3]^\circ$	$^3/_2—^5/_2$
2956,541	4	21,37	25,56	$3d'\ ^2D—(^3P_1)\ 5f\ [4]^\circ$	$^5/_2—^7/_2$
2955,388	10	19,68	23,87	$4p\ ^2D^\circ—4d\ ^2D$	$^5/_2—^5/_2$
2947,275	2	21,37	25,57	$3d'\ ^2D—(^3P_1)\ 5f\ [3]^\circ$	$^5/_2—^5/_2$
2942,892	20	17,14	21,35	$4s\ ^2P—4p'\ ^2P^\circ$	$^3/_2—^3/_2$
2941,893	1	19,68	23,89	$4p\ ^2D^\circ—4d\ ^2D$	$^5/_2—^3/_2$
2935,538	3	21,14	25,36	$4p'\ ^2F^\circ—5d\ ^2D$	$^7/_2—^5/_2$
2932,589	8	17,26	21,49	$4s\ ^2P—4p'\ ^2D^c$	$^1/_2—^3/_2$
2931,483	9	21,67	25,90	$3d'\ ^2P—(^1D)\ 4f\ [2]^c$	$^1/_2—^3/_2$
2924,642	10	21,62	25,86	$3d'\ ^2P—(^1D)\ 4f\ [1]^\circ$	$^3/_2—^3/_2$
2915,967	1	19,64	23,89	$4p\ ^4D^\circ—4d\ ^2D$	$^1/_2—^3/_2$
2915,593	4	21,37	25,62	$3d'\ ^2D—(^3P_0)\ 5f\ [3]^\circ$	$^5/_2—^7/_2$
2914,932	1	21,37	25,62	$3d'\ ^2D—(^3P_0)\ 5f\ [3]^\circ$	$^5/_2—^5/_2$
2897,332	6	21,62	25,90	$3d'\ ^2P—(^3P_2)\ 7p\ [2]^\circ$	$^3/_2—^5/_2$
2896,753	10	21,62	25,90	$3d'\ ^2P—(^1D)\ 4f\ [2]^\circ$	$^3/_2—^5/_2$
2896,564	2	21,62	25,90	$3d'\ ^2P—(^1D)\ 4f\ [2]^\circ$	$^3/_2—^3/_2$
2893,985	1	19,61	23,89	$4p\ ^4D^\circ—4d\ ^2D$	$^3/_2—^3/_2$
2891,612	18	17,14	21,43	$4s\ ^2P—4p'\ ^2P^\circ$	$^3/_2—^1/_2$
2879,327	4	—	—	—	—
2874,583	3	19,97	24,28	$4p\ ^2S^\circ—5s'\ ^2D$	$^1/_2—^3/_2$
2871,399	1	19,97	24,28	$4p\ ^4S^\circ—5s'\ ^2D$	$^3/_2—^5/_2$
2871,022	1	21,13	25,44	$4p'\ ^2F^\circ—5d\ ^2P$	$^5/_2—^3/_2$
2869,283	1	21,62	25,94	$3d'\ ^2P—(^1D)\ 4f\ [3]^c$	$^3/_2—^5/_2$
2865,841	4	19,55	23,87	$4p\ ^4D^\circ—4d\ ^4D$	$^5/_2—^5/_2$
2860,742	3	20,74	25,07	$4s''\ ^2S—6p\ ^4P^\circ$	$^1/_2—^3/_2$
2847,816	3	17,14	21,49	$4s\ ^2P—4p'\ ^2D^\circ$	$^3/_2—^3/_2$
2847,146	2	20,74	25,10	$4s''\ ^2S—6p\ ^4P^\circ$	$^1/_2—^1/_2$
2844,129	4	17,14	21,50	$4s\ ^2P—4p'\ ^2D^\circ$	$^3/_2—^5/_2$
2843,369	3	20,74	25,10	$4s''\ ^2S—6p\ ^4D^c$	$^1/_2—^3/_2$
2806,168	5	19,87	24,28	$4p\ ^2P^\circ—5s'\ ^2D$	$^3/_2—^5/_2$
2805,990	1	19,87	24,28	$4p\ ^2P^c—5s'\ ^2D$	$^3/_2—^3/_2$
2800,919	1	21,67	26,10	$3d'\ ^2P—(^3P_2)\ 6f\ [2]^c$	$^1/_2—^3/_2$
2795,425	2	21,43	25,86	$3d'\ ^2D—(^1D)\ 4f\ [1]^\circ$	$^3/_2—^1/_2$
		21,43	25,86	$3d'\ ^2D—(^1D)\ 4f\ [1]^\circ$?	$^3/_2—^3/_2$
2795,289	2	21,67	26,11	$3d'\ ^2P—(^3P_2)\ 6f\ [1]^c$	$^1/_2—^3/_2$
2774,099	2	20,74	25,21	$4s''\ ^2S—6p\ ^2D^c$	$^1/_2—^3/_2$
2772,740	2	21,62	26,09	$3d'\ ^2P—(^3P_2)\ 6f\ [3]^\circ$	$^3/_2—^5/_2$
2769,748	4	21,43	25,90	$3d'\ ^2D—(^1D)\ 4f\ [2]^\circ$	$^5/_2—^3/_2$
2767,945	2	21,62	26,10	$3d'\ ^2P—(^3P_2)\ 6f\ [2]^\circ$	$^3/_2—^5/_2$
2764,648	4	19,80	24,28	$4p\ ^2P^\circ—5s'\ ^2D$	$^1/_2—^3/_2$
2763,520	1	21,62	26,11	$3d'\ ^2P—(^3P_2)\ 6f\ [1]^\circ$	$^3/_2—^3/_2$
2757,304	3	21,37	25,86	$3d'\ ^2D—(^1D)\ 4f\ [1]^c$	$^3/_2—^3/_2$
2754,864	2	16,64	21,14	$4s\ ^4P—4p'\ ^2F^c$	$^5/_2—^7/_2$
2744,797	6	21,43	25,94	$3d'\ ^2D—(^1D)\ 4f\ [3]^c$	$^3/_2—^5/_2$
2741,962	1	21,35	25,87	$4p'\ ^2P^\circ—6d\ ^4F$	$^5/_2—^5/_2$
2741,067	2	19,76	24,28	$4p\ ^2D^\circ—5s'\ ^2D$	$^3/_2—^5/_2$
2740,912	1	19,76	24,28	$4p\ ^2D^\circ—5s'\ ^2D$	$^3/_2—^3/_2$
2740,333	1	21,35	25,87	$4p'\ ^2P^\circ—6d\ ^4P$	$^5/_2—^3/_2$
2733,022	4	21,37	25,90	$3d'\ ^2D—(^3P_2)\ 7p\ [2]^\circ$	$^5/_2—^5/_2$
2732,504	6	21,37	25,90	$3d'\ ^2D—(^1D)\ 4f\ [2]^\circ$	$^5/_2—^5/_2$
2732,335	1	21,37	25,90	$3d'\ ^2D—(^1D)\ 4f\ [2]^\circ$	$^5/_2—^3/_2$
2731,639	1	21,43	25,96	$4p'\ ^2P^\circ—6d\ ^2D$	$^1/_2—^3/_2$
2720,184	2	21,67	26,23	$3d'\ ^2P—(^3P_1)\ 6f\ [2]^\circ$	$^1/_2—^3/_2$
2716,860	2	—	—	—	—

Table 5. Principal Emission Lines for Neutral and Ionized Argon in the Wavelength Interval 2600-3000A (Ref. 9)

Ar II

λ, Å	I	E_H, eV	E_B, eV	Transition	J
2708,272	6	21,37	25,94	$3d'\ ^3D—(^1D)\ 4f\ [3]^\circ$	$^5/_2—^7/_2$
2708,052	2	21,37	25,94	$3d'\ ^3D—(^1D)\ 4f\ [3]^\circ$	$^5/_2—^5/_2$
2701,719	2	—	—	—	—
2692,596	5	16,75	21,35	$4s\ ^4P—4p'\ ^2P^\circ$	$^3/_2—^3/_2$
2690,033	2	21,35	25,96	$4p'\ ^2P^\circ—6d\ ^2F$	$^3/_2—^5/_2$
2689,093	2	21,62	26,23	$3d'\ ^2P—(^3P_1)\ 6f\ [2]^\circ$	$^3/_2—^5/_2$
2687,395	1	21,35	25,96	$4p'\ ^2P^\circ—6d\ ^2D$	$^3/_2—^3/_2$
2686,322	2	16,81	21,43	$4s\ ^4P—4p'\ ^2P^\circ$	$^1/_2—^1/_2$
2683,094	3	21,62	26,24	$3d'\ ^2P—(^3P_1)\ 6f\ [3]^\circ$	$^3/_2—^5/_2$
2674,170	2	21,35	25,98	$4p'\ ^2P^\circ—6d\ ^2P$	$^3/_2—^3/_2$
2656,303	2	21,43	26,09	$3d'\ ^2D—(^3P_2)\ 6f\ [3]^\circ$	$^3/_2—^5/_2$
2654,056	2	21,62	26,29	$3d'\ ^2P—(^3P_0)\ 6f\ [3]^\circ$	$^3/_2—^5/_2$
2652,899	1	21,43	26,10	$3d'\ ^2D—(^3P_2)\ 6f\ [2]^\circ$	$^3/_2—^3/_2$
2651,906	2	21,43	26,10	$3d'\ ^2D—(^3P_2)\ 6f\ [2]^\circ$	$^3/_2—^5/_2$
2649,599	2	16,75	21,43	$4s\ ^4P—4p'\ ^2P^\circ$	$^5/_2—^1/_2$
2647,844	1	21,43	26,11	$3d'\ ^2D—(^3P_2)\ 6f\ [1]^\circ$	$^3/_2—^3/_2$
2647,247	6	19,97	24,65	$4p\ ^4S^\circ—6s\ ^4P$	$^3/_2—^5/_2$
2636,906	2	21,35	26,05	$4p'\ ^2P^\circ—6d\ ^2D$	$^3/_2—^5/_2$
2636,354	2	16,42	21,13	$3d\ ^4D—4p'\ ^2F^\circ$	$^5/_2—^5/_2$
2634,001	2	18,73	23,44	$3d\ ^2D—5p\ ^4P^\circ$	$^5/_2—^3/_2$
2627,397	3	19,97	24,69	$4p\ ^2S^\circ—6s\ ^4P$	$^1/_2—^3/_2$
		16,42	21,14	$3d\ ^4D—4p'\ ^2F^\circ$	$^5/_2—^7/_2$
2625,711	1	16,41	21,13	$3d\ ^4D—4p'\ ^2F^\circ$	$^7/_2—^5/_2$
2624,593	3	19,97	24,69	$4p\ ^4S^\circ—6s\ ^4P$	$^3/_2—^3/_2$
2623,090	1	21,37	26,09	$3d'\ ^2D—(^3P_2)\ 6f\ [4]^\circ$	$^5/_2—^7/_2$
2621,879	1	21,37	26,09	$3d'\ ^2D—(^3P_2)\ 6f\ [3]^\circ$	$^5/_2—^5/_2$
2620,985	4	21,37	26,09	$3d'\ ^2D—(^3P_2)\ 6f\ [3]^\circ$	$^5/_2—^7/_2$
2617,596	2	19,55	24,28	$4p\ ^4D^\circ—5s'\ ^2D$	$^5/_2—^5/_2$
		21,37	26,10	$3d'\ ^2D—(^3P_2)\ 6f\ [2]^\circ$	$^5/_2—^5/_2$
2616,811	3	16,41	21,14	$3d\ ^4D—4p'\ ^2F^\circ$	$^7/_2—^7/_2$
2600,956	3	19,97	24,74	$4p\ ^2S^\circ—4d'\ ^2P$	$^1/_2—^3/_2$

Ar III

λ, Å	I	E_H, eV	E_B, eV	Transition	J
2884,12	9	24,38	28,68	$4s'\ ^3D^\circ—4p'\ ^3P$	3—2
2878,72	5	24,38	28,68	$4s'\ ^3D^\circ—4p'\ ^3P$	2—2
2876,65	1	24,37	28,68	$4s'\ ^3D^\circ—4p'\ ^3P$	1—2
2855,29	8	24,38	28,72	$4s'\ ^3D^\circ—4p'\ ^3P$	2—1
2853,23	6	24,37	28,72	$4s'\ ^3D^\circ—4p'\ ^3P$	1—1
2842,88	7	24,37	28,73	$4s'\ ^3D^\circ—4p'\ ^3P$	1—0
2824,66	6	25,73	30,12	$4s''\ ^3P^\circ—4p''\ ^3P$	1—0
2818,26	6	25,75	30,14	$4s''\ ^3P^\circ—4p''\ ^3P$	0—1
2807,02	4	25,73	30,14	$4s''\ ^3P^\circ—4p''\ ^3P$	1—1
2785,23	5	25,73	30,18	$4s''\ ^3P^\circ—4p''\ ^3P$	1—2
2783,65	5	25,69	30,14	$4s''\ ^3P^\circ—4p''\ ^3P$	2—1
2762,23	7	25,69	30,18	$4s''\ ^3P^\circ—4p''\ ^3P$	2—2
2743,89	3	23,40	27,91	$3d'\ ^3D^\circ—4p'\ ^3D$	3—2
2724,84	10	23,40	27,94	$3d'\ ^3D^\circ—4p'\ ^3D$	3—3
2685,63	6	28,73	33,35	$4p'\ ^3P—4d'\ ^3D^\circ$	0—1
2678,38	9	23,29	27,91	$3d'\ ^3D^\circ—4p'\ ^3D$	2—2
2677,87	3	23,29	27,91	$3d'\ ^3D^\circ—4p'\ ^3D$	2—1
2676,46	4	28,72	33,35	$4p'\ ^3P—4d'\ ^3D^\circ$	1—1
2674,02	8	28,72	33,35	$4p'\ ^3P—4d'\ ^3D^\circ$	1—2
2660,22	3	23,29	27,94	$3d'\ ^3D^\circ—4p'\ ^3D$	2—3
2656,17	1	28,68	33,35	$4p'\ ^3P—4d'\ ^3D^\circ$	2—1
2654,63	10	28,68	33,35	$4p'\ ^3P—4d'\ ^3D^\circ$	2—3
2653,77	4	28,68	33,35	$4p'\ ^3P—4d'\ ^3D^\circ$	2—2
2645,47	2	23,40	28,08	$3d'\ ^3D^\circ—4p'\ ^3F$	3—3
2632,40	4	23,21	27,91	$3d'\ ^3D^\circ—4p'\ ^3D$	1—2
2631,90	7	23,21	27,91	$3d'\ ^3D^\circ—4p'\ ^3D$	1—1
2617,26	1	25,38	30,12	$3d'\ ^3S^\circ—4p''\ ^3P$	1—0
2613,95	3	23,17	27,91	$3d'\ ^3F^\circ—4p'\ ^3D$	2—2
2613,44	3	23,17	27,91	$3d'\ ^3F^\circ—4p'\ ^3D$	2—1
2602,12	1	25,38	30,14	$3d'\ ^3S^\circ—4p''\ ^3P$	1—1
2597,25	3	23,14	27,91	$3d'\ ^3F^\circ—4p'\ ^3D$	3—2
2594,41	1	23,29	28,08	$3d'\ ^3D^\circ—4p'\ ^3F$	2—3

Table 5. Principal Emission Lines for Neutral and Ionized Argon in the Wavelength Interval 2600-3000A (Ref. 9)(Continued)

Xe II

λ, A	I	E_H, eV	E_B, eV	Transition	J
2999,21	15	—	—	—	—
2991,73	3	14,07	18,22	$6p\ ^4D°—14$	$^5/_2—^5/_2$
		11,27	15,41	$5p^6\ ^2S—6p\ ^2D°$	$^1/_2—^3/_2$
2990,54	12	13,25	17,40	$5d\ ^4P—19°$	$^1/_2—^3/_2$
2986,82	8	11,83	15,98	$5d\ ^4D—6p'\ ^2F°$	$^5/_2—^5/_2$
2986,18	10	—	—	—	—
2982,23	2	—	—	—	—
2979,32	300	13,20	17,36	$5d\ ^4P—15°$	$^5/_2—^5/_2$
2977,90	5	—	—	—	—
2976,39	8	—	—	—	—
2974,86	20	13,31	17,48	$5d\ ^4P—21°$	$^3/_2—^3/_2$
2972,31	8	11,91	16,08	$5d\ ^4D—6p'\ ^2P°$	$^3/_2—^3/_2$
2969,80	12	—	—	—	—
2969,23	3	—	—	—	—
2966,74	1	11,27	15,44	$5p^6\ ^2S—6p\ ^2P°$	$^1/_2—^1/_2$
2964,19	12	—	—	—	—
2963,41	50	13,20	17,38	$5d\ ^4P—6p''\ ^2P°$	$^5/_2—^3/_2$
2955,84	2	—	—	—	—
2954,78	2	—	—	—	—
2952,48	2	13,20	17,40	$5d\ ^4P—19°$	$^5/_2—^3/_2$
2951,58	2	13,06	17,26	$5d\ ^2P—7°$	$^3/_2—^3/_2$
2949,77	4	—	—	—	—
2944,61	4	—	—	—	—
2943,41	4	—	—	—	—
2942,10	20	—	—	—	—
2941,38	8	—	—	—	—
2939,72	5	—	—	—	—
2935,86	60	—	—	—	—
2934,80	2	13,14	17,36	$5d\ ^2P—13°$	$^1/_2—^1/_2$
2933,34	1	13,25	17,48	$5d\ ^4P—21°$	$^1/_2—^3/_2$
2927,58	2	13,86	18,09	$6p\ ^4P°—6d\ ^2D$	$^3/_2—^3/_2$
2924,38	2	13,06	17,29	$5d\ ^2P—9°$	$^3/_2—^3/_2$
2923,95	6	—	—	—	—
2923,03	1	14,23	18,47	$5d'\ ^2F—33°$	$^5/_2—^7/_2$
2919,87	40	13,14	17,38	$5d\ ^2P—17°$	$^1/_2—^1/_2$
2910,64	1	13,89	18,14	$6p\ ^4P°—7s'\ ^2D$	$^5/_2—^5/_2$
2910,27	3	—	—	—	—
2907,18	80	13,14	17,40	$5d\ ^2P—19°$	$^1/_2—^3/_2$
2905,10	2	14,09	18,36	$6p\ ^4P°—6d'\ ^2D$	$^1/_2—^3/_2$
2904,18	3	—	—	—	—
2902,68	3	—	—	—	—
2895,22	150	14,23	18,51	$5d'\ ^2F—35°$	$^5/_2—^5/_2$
2889,07	10	11,79	16,08	$6s\ ^4P—6p'\ ^2P°$	$^3/_2—^3/_2$
2887,12	10	11,83	16,12	$5d\ ^4D—6p'\ ^2F°$	$^7/_2—^7/_2$
2883,71	12	11,83	16,12	$5d\ ^4D—6p'\ ^2F°$	$^5/_2—^7/_2$
2881,14	1	13,06	17,36	$5d\ ^2P—13°$	$^3/_2—^1/_2$
2871,24	50	—	—	—	—
2867,36	2	13,97	18,30	$5d'\ ^2D—29°$	$^5/_2—^3/_2$
2866,76	5	13,06	17,38	$5d\ ^2P—17°$	$^3/_2—^1/_2$
2864,73	150	13,06	17,38	$5d\ ^2P—6p''\ ^2P°$	$^3/_2—^3/_2$
2861,90	20	14,23	18,56	$5d'\ ^2F—37°$	$^5/_2—^5/_2$
2856,65	2	—	—	—	—
2854,53	60	13,06	17,40	$5d\ ^2P—19°$	$^3/_2—^3/_2$
2853,11	1	13,14	17,48	$5d\ ^2P—21°$	$^1/_2—^3/_2$
2852,39	3	—	—	—	—
2850,95	3	12,01	16,36	$5d\ ^4D—6p'\ ^2D°$	$^3/_2—^3/_2$
2849,66	8	—	—	—	—
2846,48	3	—	—	—	—
2845,92	8	—	—	—	—
2844,45	5	—	—	—	—
2839,57	2	—	—	—	—

Table 6. Principal Emission Lines for Ionized Xenon in the Wavelength Interval 2600-3000A (Ref. 9)

λ, Å	I	E_H, eV	E_B, eV	Transition	J
2838,85	3	—	—	—	—
2836,16	1	12,92	17,29	$6s\ ^2P-9°$	$^1/_2-^3/_2$
2832,46	2	—	—	—	—
2832,00	2	—	—	—	—
2827,90	2	—	—	—	—
2826,94	5	—	—	—	—
2820,06	4	14,00	18,40	$6s'\ ^2D-31°$	$^3/_2-^3/_2$
2819,02	1	13,39	17,79	$6s'\ ^2D-23°$	$^5/_2-^3/_2$
2808,56	4	—	—	—	—
2807,55	2	—	—	—	—
2803,02	5	—	—	—	—
2802,50	1	13,97	18,40	$5d'\ ^2D-31°$	$^5/_2-^3/_2$
2797,65	30	12,59	17,02	$5d\ ^4F-1°$	$^5/_2-^3/_2$
2796,49	2	—	—	—	—
2792,52	1	11,54	15,98	$6s\ ^4P-6p'\ ^2F°$	$^5/_2-^5/_2$
2789,52	2	—	—	—	—
2785,42	3	11,91	16,36	$5d\ ^4D-6p'\ ^2D°$	$^3/_2-^3/_2$
2782,73	2	—	—	—	—
2774,86	15	14,00	18,47	$6s'\ ^2D-33°$	$^3/_2-^3/_2$
2773,55	5	—	—	—	—
2770,41	2	12,92	17,40	$6s\ ^2P-19°$	$^1/_2-^3/_2$
2767,00	1	14,09	18,57	$6p\ ^4P°-7s'\ ^2D$	$^1/_2-^3/_2$
2763,56	1	11,91	16,39	$5d\ ^4D-6p'\ ^2D'$	$^3/_2-^5/_2$
2762,77	2	14,07	18,56	$6p\ ^4D°-6d'\ ^2D$	$^5/_2-^5/_2$
2758,36	1	13,80	18,30	$5d'\ ^2D-29°$	$^3/_2-^3/_2$
2757,86	40	13,97	18,47	$5d'\ ^2D-33°$	$^5/_2-^3/_2$
2744,04	2	—	—	—	—
2743,16	2	—	—	—	—
2734,14	50	13,25	17,79	$5d\ ^4P-23°$	$^1/_2-^3/_2$
2733,15	25	13,97	18,51	$5d'\ ^2D-35°$	$^5/_2-^5/_2$
2731,46	1	11,54	16,08	$6s\ ^4P-6p'\ ^2P°$	$^5/_2-^3/_2$
2723,40	1	11,91	16,46	$5d\ ^4D-6p'\ ^2P°$	$^3/_2-^1/_2$
2721,28	1	12,92	17,48	$6s\ ^2P-21°$	$^1/_2-^3/_2$
2718,79	1	11,83	16,39	$5d\ ^4D-6p'\ ^2D°$	$^7/_2-^5/_2$
2717,35	30	—	—	—	—
2715,76	3	11,83	16,39	$5d\ ^4D-6p'\ ^2D°$	$^5/_2-^5/_2$
2703,44	10	13,97	18,56	$5d'\ ^2D-37°$	$^5/_2-^5/_2$
2702,34	2	13,20	17,79	$5d\ ^4P-23°$	$^5/_2-^3/_2$
2702,22	2	11,54	16,12	$6s\ ^4P-6p'\ ^2F°$	$^5/_2-^7/_2$
2691,40	1	11,79	16,39	$6s\ ^4P-6p'\ ^2D°$	$^3/_2-^5/_2$
2687,03	5	—	—	—	—
2686,14	3	14,76	19,38	$5d''\ ^2D-39°$	$^5/_2-^3/_2$
2677,18	50	—	—	—	—
2672,22	4	12,74	17,38	$6s\ ^2P-6p''\ ^2P°$	$^3/_2-^3/_2$
2668,02	5	12,59	17,23	$5d\ ^4F-3°$	$^5/_2-^7/_2$
2663,29	3	12,74	17,40	$6s\ ^2P-19°$	$^3/_2-^3/_2$
2659,28	1	12,59	17,25	$5d\ ^4F-5°$	$^5/_2-^3/_2$
2657,00	5	13,80	18,47	$5d'\ ^2D-33°$	$^3/_2-^3/_2$
2655,39	2	—	—	—	—
2634,20	2	—	—	—	—
2633,88	2	13,58	18,29	$5d\ ^2D-25°$	$^5/_2-^3/_2$
2631,25	2	11,27	15,98	$5p^6\ ^2S-6p'\ ^2F°$	$^1/_2-^5/_2$
2630,40	6	13,58	18,30	$5d\ ^2D-29°$	$^5/_2-^3/_2$
2629,54	5	—	—	—	—
2621,39	2	—	—	—	—
2607,52	1	12,54	17,29	$6s\ ^4P-9°$	$^1/_2-^3/_2$
2606,93	5	—	—	—	—
2605,54	50	—	—	—	—

Table 6. Principal Emission Lines for Ionized Xenon in the Wavelength Interval 2600-3000A (Ref. 9) (Continued)

Xe III

λ, Å	I	E_H, eV	E_B, eV	Transition	J
2994,69	8	20,16	24,30	$6p'\ ^3F-31°$	3—2
2992,91	40	18,48	22,62	$6p\ ^5P-6d\ ^5D°$	3—3
2991,45	8	16,70	20,84	$6s'\ ^3D°-6p'\ ^3P$	2—1
2991,25	10	18,48	22,62	$6p\ ^5P-6d\ ^5D°$	3—2
2984,63	15	20,65	24,80	$6p'\ ^3F-39°$	4—3
2971,24	8	16,52	20,69	$6s'\ ^3D°-6p'\ ^3P$	1—2
2969,45	4	20,16	24,33	$6p'\ ^3F-33°$	3—2, 3
2968,56	10	20,63	24,80	$6p'\ ^3D-39°$	3—3
2966,97	10	20,62	24,80	$4f'\ 6-39°$	4—3
2964,98	15	20,12	24,30	$6p'\ ^3D-31°$	2—2
2948,06	40	15,91	20,12	$5d'\ ^3F°-6p'\ ^3D$	2—2
2947,53	40	16,42	20,62	$5d'\ ^1G°-4f'\ 6$	4—4
2945,25	60	20,16	24,37	$6p'\ ^3F-35°$	3—2, 3
2940,22	40	20,12	24,33	$6p'\ ^3D-33°$	2—2, 3
2939,13	10	20,16	24,38	$6p'\ ^3F-37°$	3—2, 3
2932,74	25	13,97	18,24	$5d\ ^5D°-6p\ ^5P$	0—1
2930,29	20	16,42	20,65	$5d'\ ^1G°-6p'\ ^3F$	4—4
2923,51	25	16,38	20,62	$5d'\ ^3G°-4f'\ 6$	4—4
2917,59	20	16,14	20,39	$5d'\ ^3G°-6p'\ ^1F$	3—3
2914,12	20	15,46	19,71	$5d\ ^3D°-6p'\ ^3D$	2—1
2911,90	40	13,94	18,20	$5d\ ^5D°-6p\ ^5P$	1—1
2911,47	2	18,32	22,58	$3d''\ 13°-6p''\ 28$	1—1
2906,56	50	16,38	20,65	$5d'\ ^3G°-6p'\ ^3F$	4—4
2899,57	1	15,84	20,12	$5d'\ ^1F°-6p'\ ^3D$	3—2
2897,69	2	17,45	21,72	$5d'\ ^3S°-6p\ ^3D$	1—1
2896,63	30	13,94	18,22	$5d\ ^5D°-6p\ ^5P$	1—2
2891,71	25	15,64	19,92	$5d'\ ^3F°-6p'\ ^3F$	3—2
2872,73	2	17,75	22,06	$5d'\ ^3D°-6p''\ ^3D$	3—2
2871,68	30	15,84	20,16	$5d'\ ^1F°-6p'\ ^3F$	3—3
2868,42	1	16,52	20,84	$6s'\ ^3D°-6p'\ ^3P$	1—1
2863,86	1	17,73	22,06	$6s'\ ^1D°-6p''\ ^3D$	2—2
2862,41	30	13,87	18,20	$5d\ ^5D°-6p\ ^5P$	2—1
2857,81	1	17,73	22,07	$6s'\ ^1D°-6p''\ 26$	2—1
2850,25	2	15,57	19,92	$6s\ ^3S°-6p'\ ^3F$	1—2
2847,66	40	13,87	18,22	$5d\ ^5D°-6p\ ^5P$	2—2
2839,57	2	19,92	24,29	$6p'\ ^3F-29°$	2—2
2624,52	1	18,32	23,05	$5d''\ 13°-6p''\ 36$	1—1, 2
2608,90	6	15,64	20,39	$5d'\ ^3F°-6p'\ ^1F$	3—3
2838,85	3	18,94	23,31	$6p\ ^3P-7s\ ^3S°$	0—1
2833,18	6	19,92	24,30	$6p'\ ^3F-31°$	2—2
2832,95	6	17,19	21,57	$6s'\ ^3D°-6p''\ ^3D$	3—3
2827,45	30	13,84	18,22	$5d\ ^5D°-6p\ ^5P$	3—2
2826,05	20	18,22	22,61	$6p\ ^5P-7s\ ^5S°$	2—2
2815,94	40	18,22	22,62	$6p\ ^5P-6d\ ^5D°$	2—3
2814,47	30	18,22	22,62	$6p\ ^5P-6d\ ^5D°$	2—2
2811,67	8	18,20	22,61	$6p\ ^5P-7s\ ^5S°$	1—2
2810,52	1	19,92	24,33	$6p'\ ^3F-33°$	2—2, 3
2809,07	8	18,22	22,63	$6p\ ^5P-6d\ ^5D°$	2—1
2807,25	10	20,39	24,80	$6p'\ ^1F-39°$	3—3
2806,39	3	16,91	21,32	$5d'\ 41°-6p'\ ^1D$	2—2
2805,08	2	18,39	22,81	$5d''\ 15°-6p''\ 32$	2—1
2800,22	20	18,20	22,62	$6p\ ^5P-6d\ ^5D°$	1—2
2794,86	20	18,20	22,63	$6p\ ^5P-6d\ ^5D°$	1—1
2783,37	12	19,92	24,38	$6p'\ ^3F-37°$	2—2, 3
2779,64	5	18,85	23,31	$6p\ ^3P-7s\ ^3S°$	2—1
		17,61	22,07	$5d'\ ^3D°-6p''\ 26$	2—1
2776,96	10	15,46	19,92	$5d\ ^3D°-6p'\ ^3F$	2—2
2772,41	10	18,20	22,67	$6p\ ^5P-6d\ ^5D°$	1—0
2766,20	5	15,64	20,12	$5d'\ ^3F°-6p'\ ^3D$	3—2
2763,00	1	16,14	20,62	$5d'\ ^3G°-4f'\ 6$	3—4
2761,60	12	18,39	22,88	$5d''\ 15°-6p''\ 34$	2—1
		16,14	20,63	$5d'\ ^3G°-6p'\ ^3D$	3—3
2760,76	6	18,32	22,81	$5d''\ 13°-6p''\ 32$	1—1
2747,88	8	16,14	20,63	$5d'\ ^3G°-6p'\ ^3F$	3—4
2740,80	12	15,64	20,16	$5d'\ ^3F°-6p'\ ^3F$	3—3
2728,22	4	15,57	20,12	$6s\ ^2S°-6p'\ ^3D$	1—2
2727,22	4	15,84	20,39	$5d'\ ^1F°-6p'\ ^1F$	3—3
2696,50	8	15,12	19,71	$5d\ ^3D°-6p'\ ^3D$	1—1
2687,03	5	13,87	18,46	$5d\ ^5D°-6p\ ^5P$	2—3
2685,58	2	17,45	22,06	$5d'\ ^3S°-6p''\ ^3D$	1—2
2678,54	1	16,70	21,32	$6s'\ ^3D°-6p'\ ^1D$	2—2
2669,00	10	13,84	18,48	$5d\ ^5D°-6p\ ^5P$	3—3
2661,00	1	15,46	20,12	$5d\ ^3D°-6p'\ ^3D$	2—2
2658,26	3	13,97	18,63	$5d\ ^5D°-6p\ ^3P$	0—1
2650,20	1	18,63	23,31	$6p\ ^3P-7s\ ^3S°$	1—1
2641,12	5	13,94	18,63	$5d\ ^5D°-6p\ ^3P$	1—1
2637,54	3	15,46	20,16	$5d\ ^3D°-6p'\ ^3F$	2—3

Table 6. Principal Emission Lines for Ionized Xenon in the Wavelength Interval 2600-3000A (Ref. 3) (Continued)

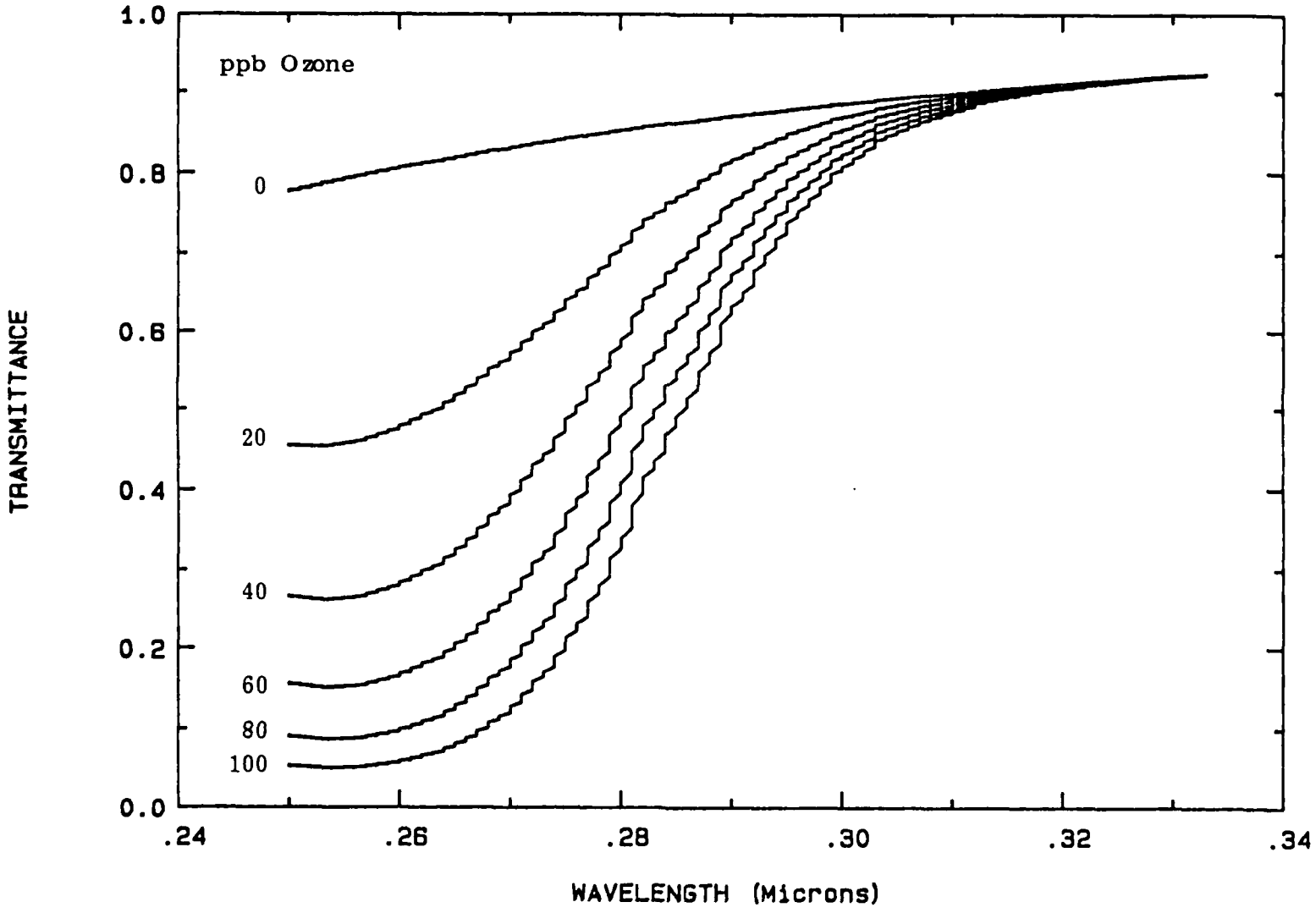

Figure 4. Atmospheric Transmittance for 1 km Range
0.0 to 100 ppb Ozone

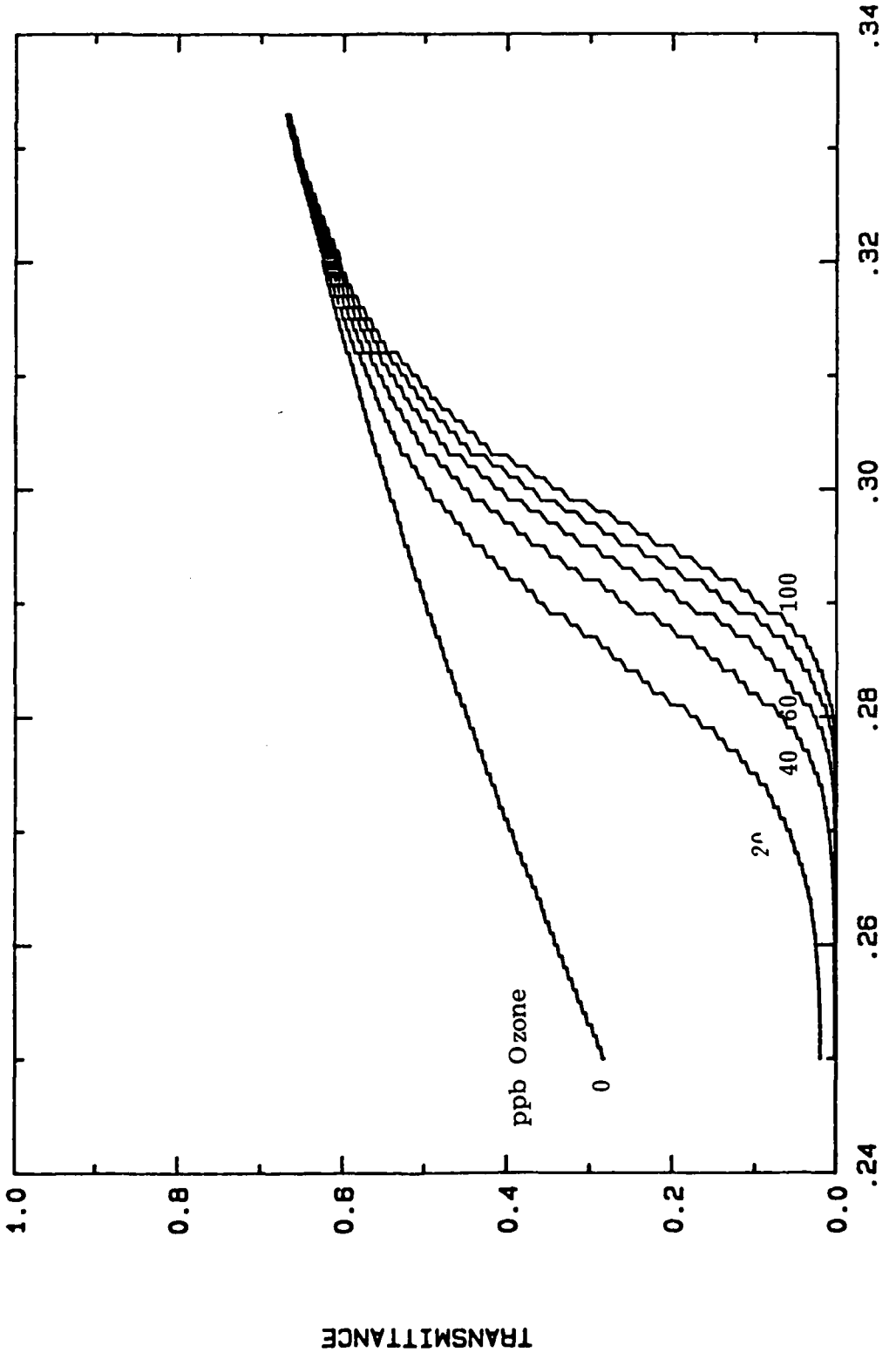

Figure 5. Atmospheric Transmittance for 5 km Range
0.0 to 100 ppb Ozone

naturally focussed increasingly on the upper end of the solar blind region. Much of our prior interest in the possibility of exploiting the extreme power efficiencies displayed by low pressure Hg lamps, therefore was shown to have been in vain. Subsequently, other candidate emitters were investigated which it was hoped could be made to radiate in the more transparent regions of the upper solar blind bandpass.

3. APPARATUS

3.1 Experimental Flashlamps

The desire to change gas mixtures and electrodes spacings often and quickly made it extremely impractical to have a number of conventional lamps fabricated for each parametric variation to be examined. A somewhat cumbersome but highly versatile flashlamp design was therefore conceived as indicated in Figure 6 from two commercially available Cajon vacuum fittings and a 1.8 centimeter silica tube. Provision was made for emptying or refilling the lamp tube through a 0.6 centimeter diameter opening at one end of the apparatus and O-ring sealed feed throughs were employed at each of the two ends to facilitate movement of tapered tungsten electrodes mounted on the ends of 1.6 mm diameter rods.

The trigger electrode comprising a 0.1 mm diameter wire rested against the inside wall of the discharge tube and connected to the high voltage anode. The trigger electrode ground ring was painted on the outside of the tube opposite the end of the trigger electrode. The entire configuration was designed to allow both electrodes to be electrically isolated from all other components of the system.

3.2 Gas Handling System

A schematic of the vacuum train and gas handling system is presented in Figure 7. The entire apparatus is fabricated from Pyrex glass, stainless steel and high vacuum fittings. It is capable of being evacuated to below 10^{-7} Torr. The pumping was provided by a Varian model HS-2, 2 inch diameter oil diffusion pump backed by an Alcatel model ZM 2004A 250 l/min mechanical pump. Pressure measurements were made using manometers, a McLeod gauge which was interchangeable with the manometer, and a Datametrics barocel passidence capacitance manometer manifolded to a number of points throughout the system.

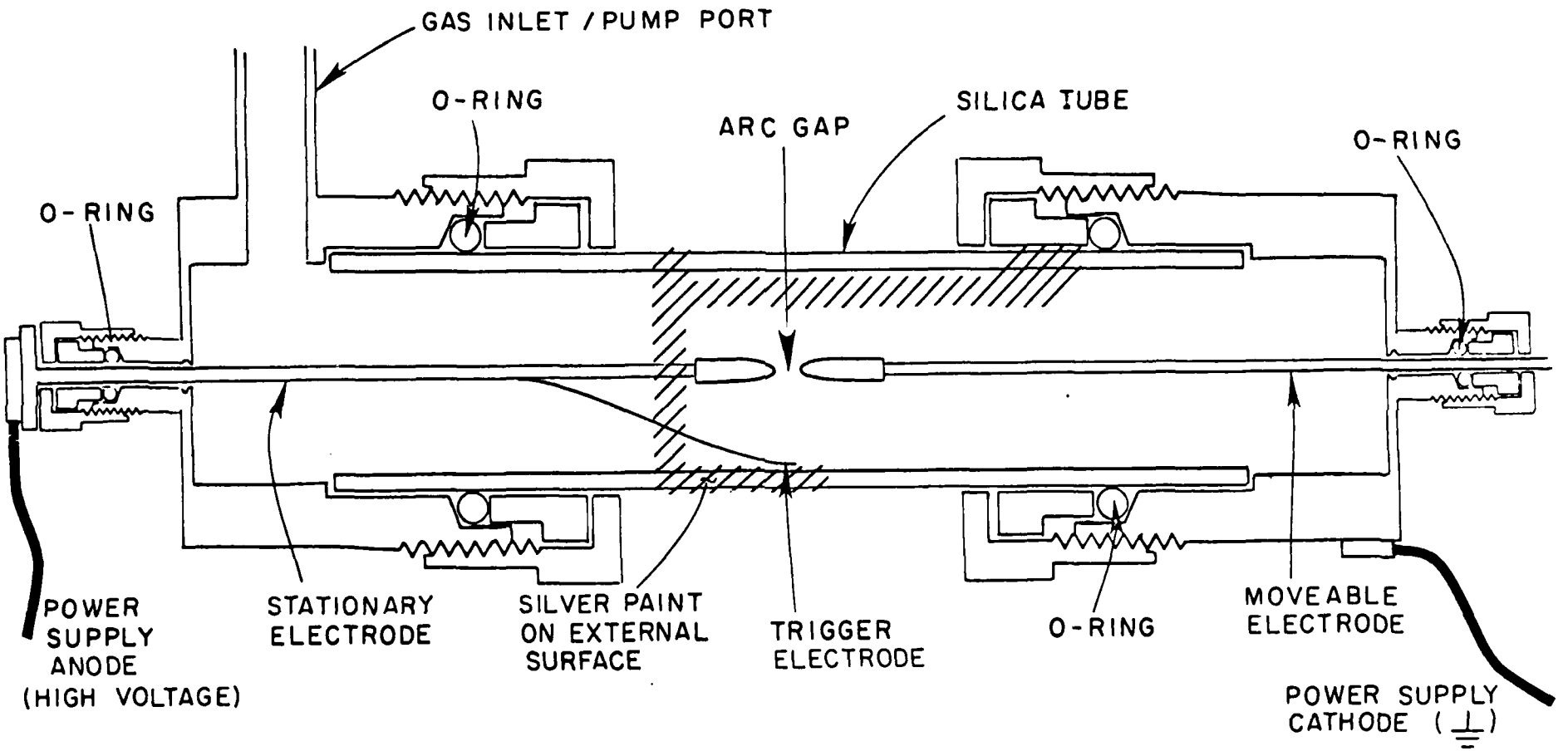

Figure 6. Laboratory Flash Lamp

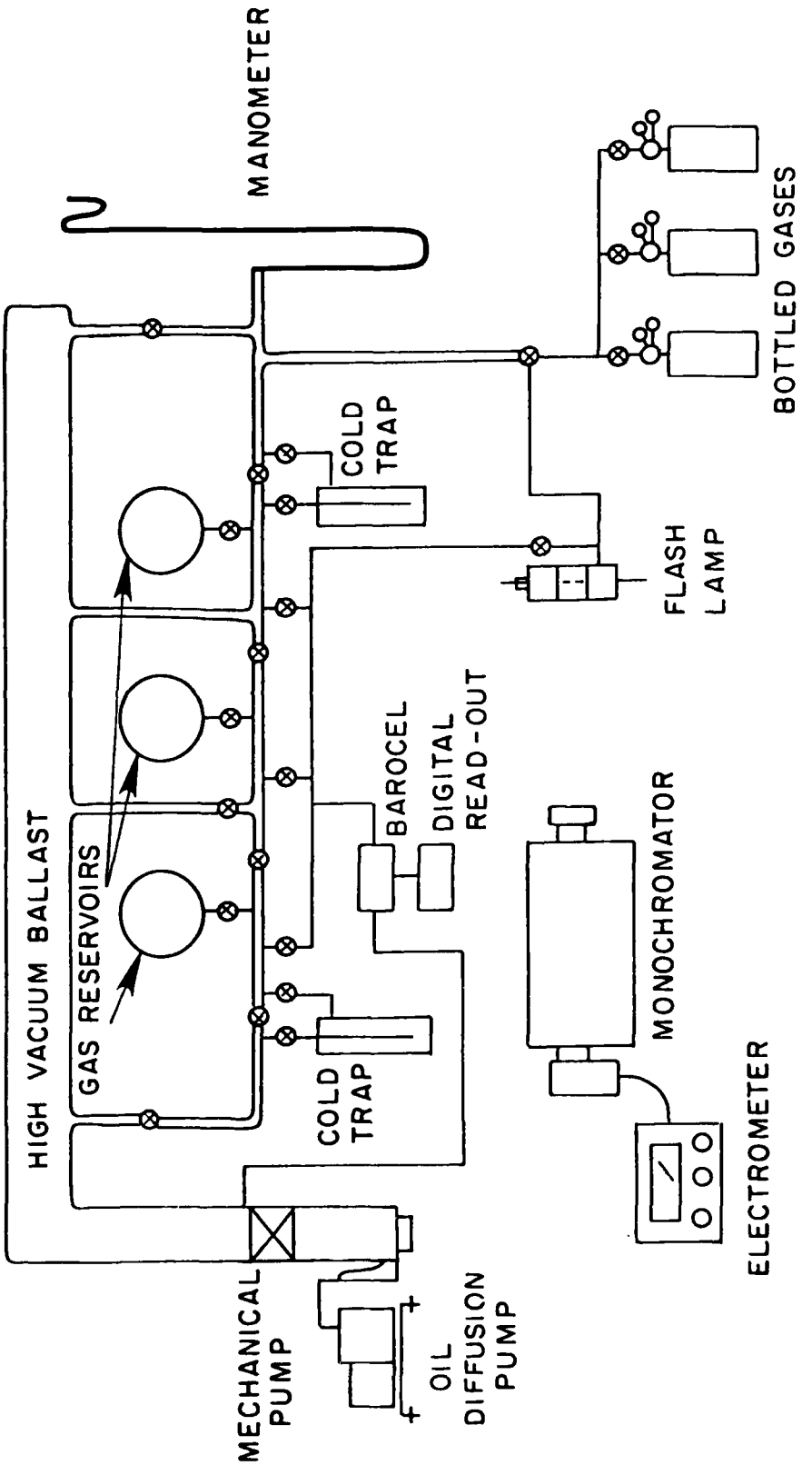

Figure 7. Gas Handling Apparatus

The different sized storage reservoirs and the cold traps used to hold condensed gases at liquid nitrogen temperatures provided means of preparing mixtures of various gases in any desired proportions. The entire system was accessible to a high pumping speed, low pressure manifold at a number of points along the train at the approximate locations indicated in Figure 7. Seals between the glass gas handling system and the stainless steel vacuum manifold were made with compression fittings equipped with high vacuum O rings.

3.3 Electro Optics

Spectrally resolved information on the various lamp emissions was obtained using a model HR320 Instruments SA F/4.8 spectrograph with a 2400 g/mm grating blazed at 300 nm. The maximum resolution of this instrument is about 0.05 nm at 300 nm. A Hamamatsu R106 photomultiplier tube served as the detector both in this instrument and in a radiometer equipped with interchangeable filters. The bandpasses of the several filters used in this study are given in Figure 8. These filter transmission characteristics as well as the throughput efficiency of the spectrograph as a function of wavelength were determined using a D_2 discharge lamp as an absolute calibration standard. The output of this lamp is given in Figure 9; it was obtained from Optronic Laboratories, Inc. and is traceable to NBS standards. The resultant throughput curve for the monochrometer/PMT combination is presented in Figure 10. This data is normalized to the maximum sensitivity value which occurs at about 325 nm.

3.4 Electronics

A power supply to drive the experimental test lamp was designed and built specifically for the purposes of this study. The requirements of the program called for a high degree of flexibility in a number of electrical parameters including frequency, voltage, capacitance and holdoff time.

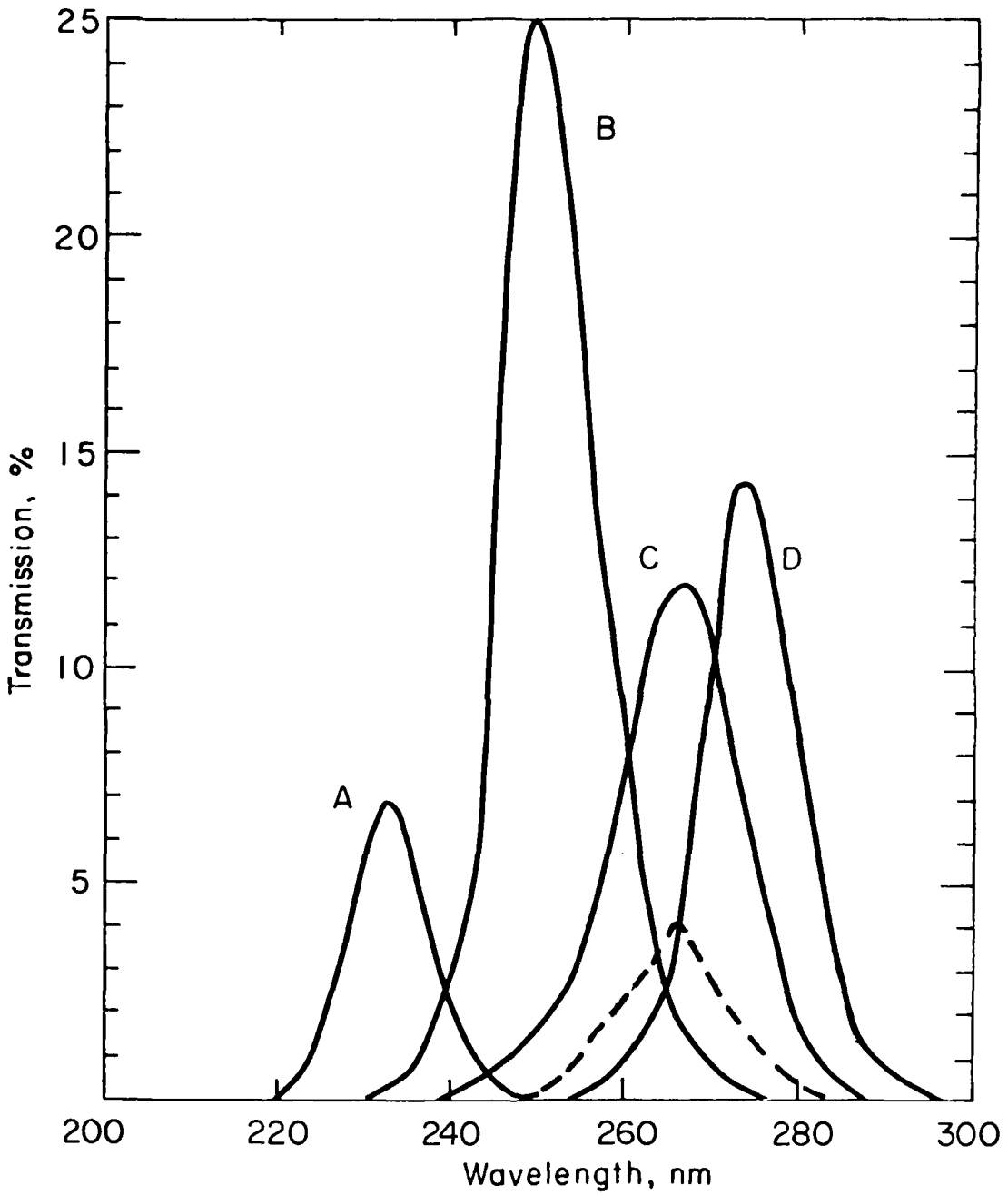

Figure 8. Transmission Characteristics of Solar Blind Filters Used

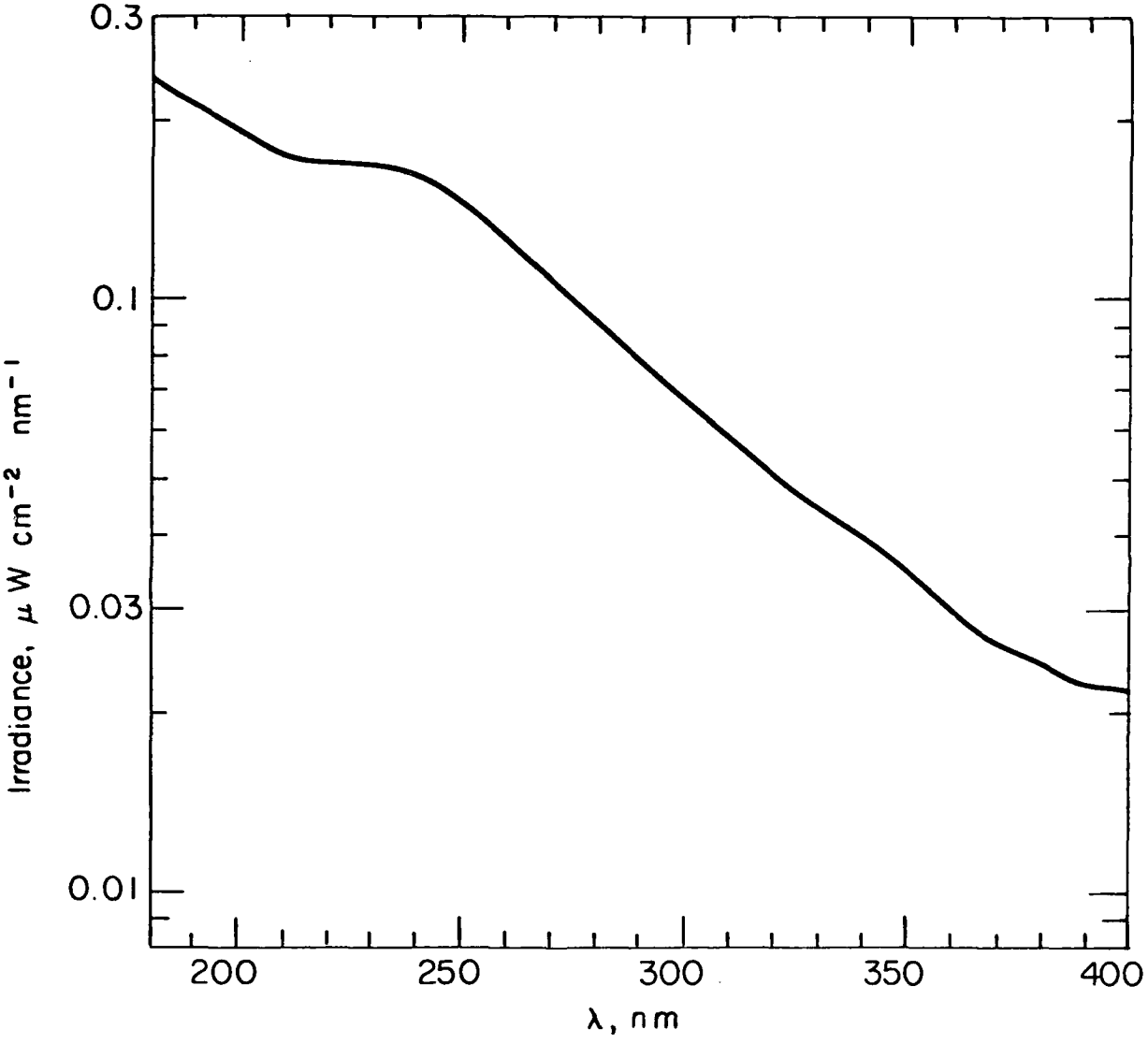

Figure 9. Standard Lamp Output
500 mA, 30 cm distance

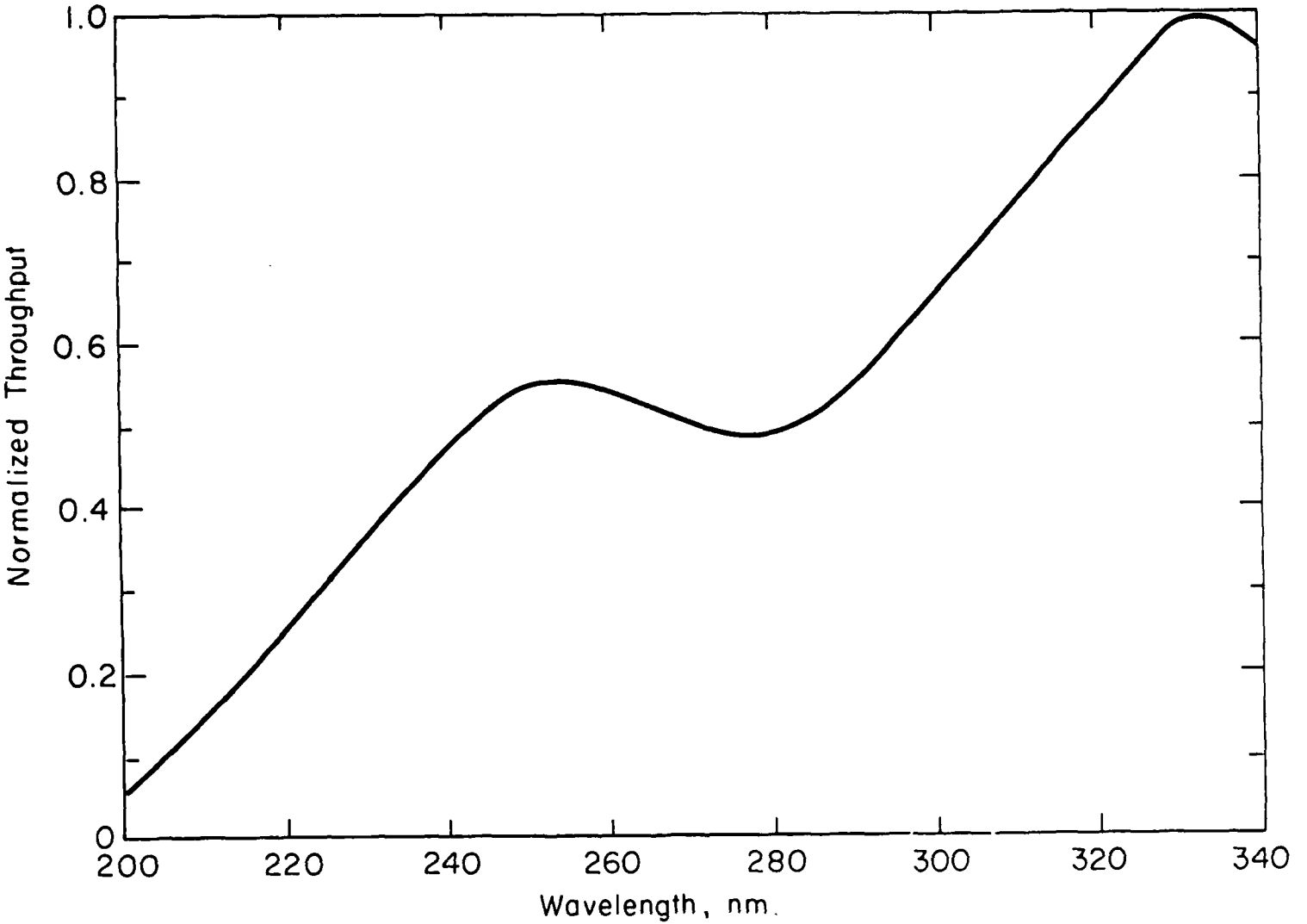

Figure 10. Monochrometer/PMT Wavelength Response Curve

Practical considerations made it impossible to achieve all of our design objectives in one piece of equipment. The device eventually built, which resulted from a compromise between our wishes and our resources -- and which consumed a much larger proportion of the time and money available than originally anticipated -- is depicted schematically in Figure 11.

Timing for the discharge and capacitor recharging is controlled by a clock module equipped with external thumbwheel dials for frequency selection. This built-in clock module also provides an accurate frequency reference for control of the holdoff interval between pulses. The clock and holdoff timing modules, together with the recharge driver circuit which they control, and a common power supply module are contained in a "control chassis" separated and isolated from the "head chassis" power circuit enclosure which abuts the lamp itself. It proved impossible to include the trigger and main power modules in the same enclosure as the control circuits. Noise from the power circuits apparently confused the logic functions in the clock and/or timing modules and produced erratic behavior.

The clock, holdoff timing and recharge driver module details are presented in Figures 12, 13, and 14, respectively. The discharge frequency is controlled by the clock and is continuously variable from 0-30 kHz. A set of thumbwheel switches for frequency selection are provided on the face of the control unit. Provision is also made for bypassing the internal clock and triggering the device with an external signal. The recharge holdoff unit provides a controllable time interval between the end of one discharge pulse and the beginning of the capacitor recharge operation for the next pulse. During this interval, no power is applied to the lamp driver circuits and the ionized gas between the electrodes remains undisturbed and free to relax. This precludes premature breakdown which might otherwise occur as the trigger and main capacitors are being recharged. The duration of the holdoff interval is selectable via an

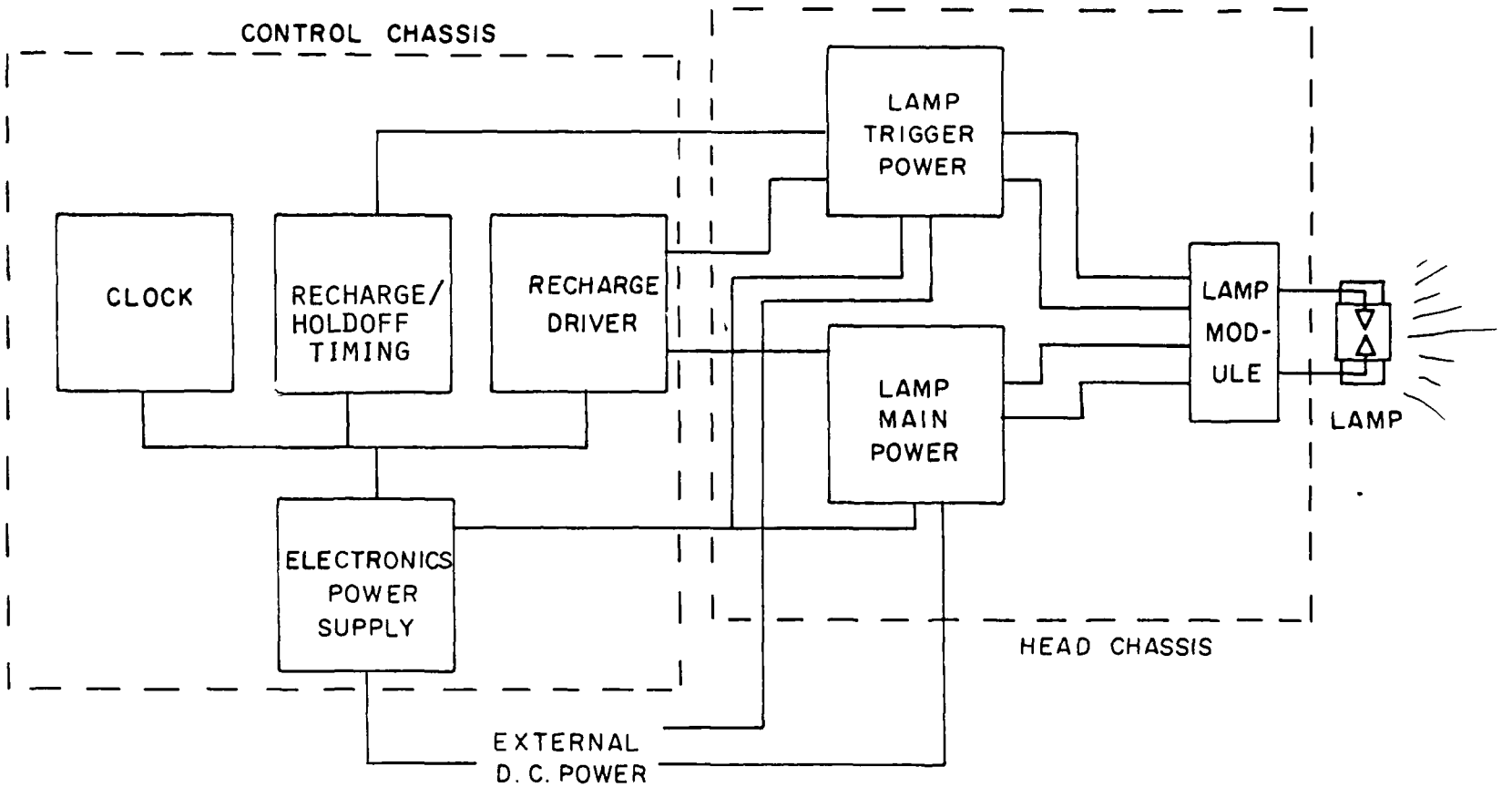

Figure 11. Lamp Power Supply Diagram

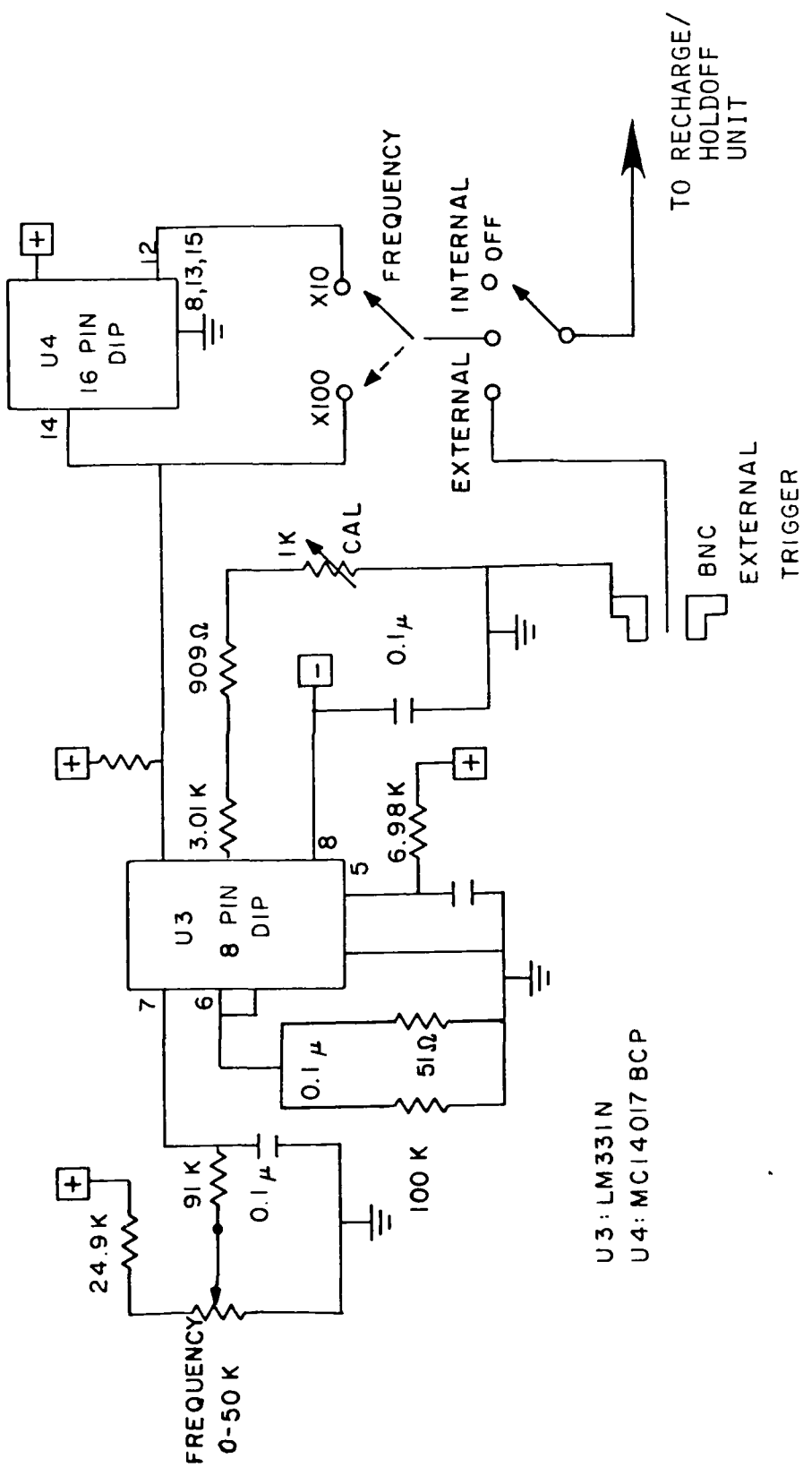

Figure 12. Clock Module Schematic

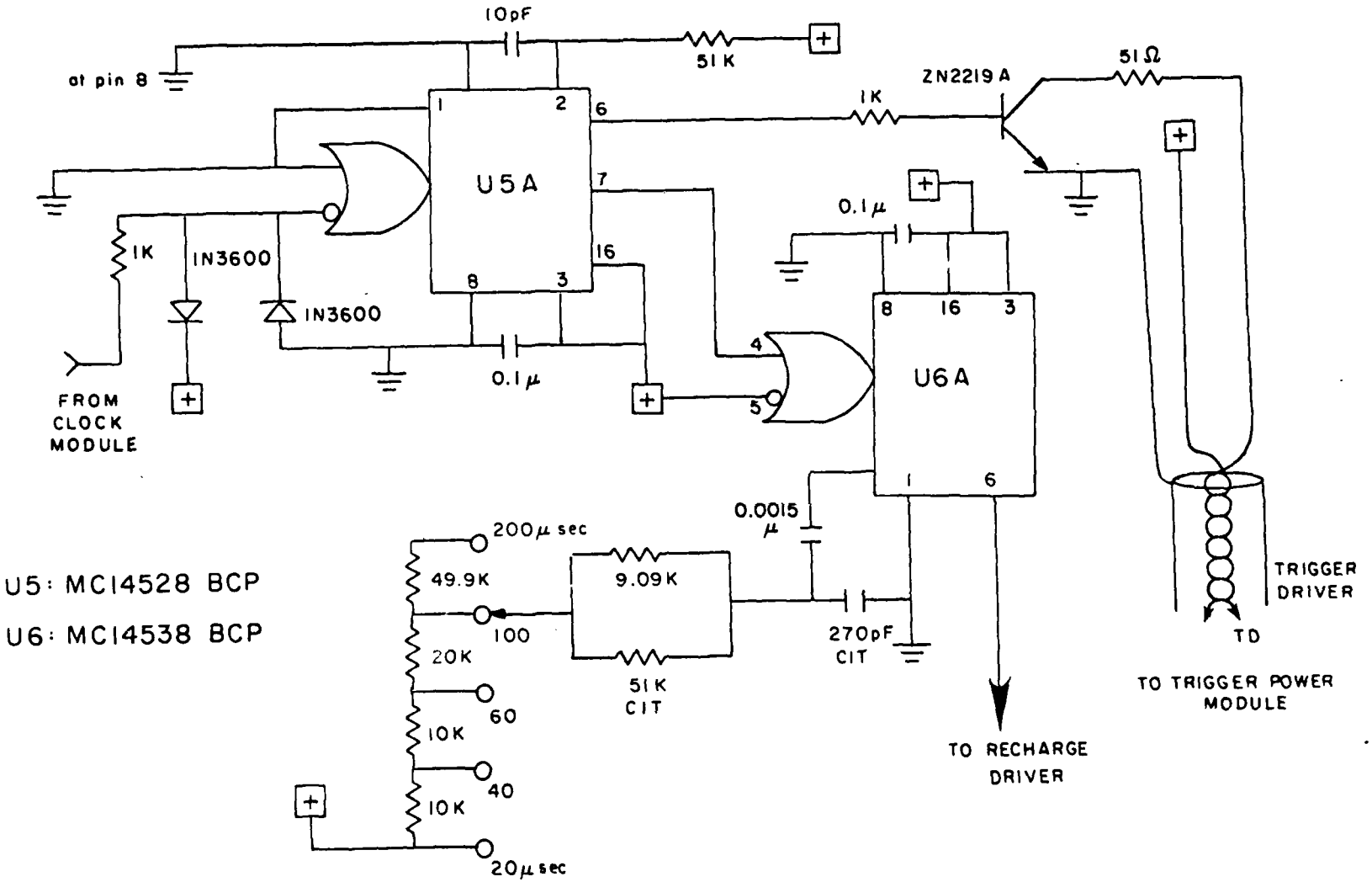

Figure 13. Recharge/Holdoff Timing Module Schematic

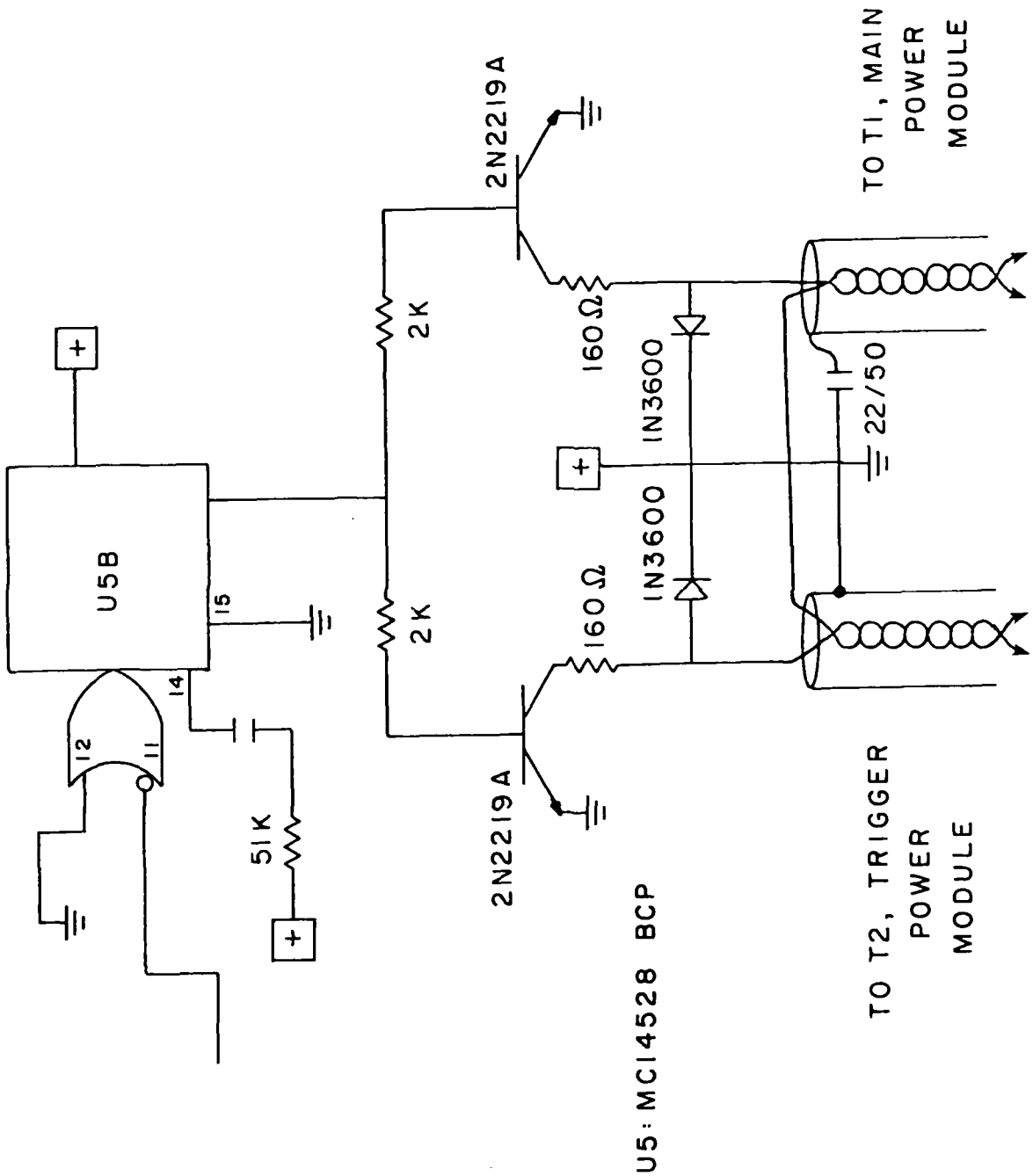

Figure 14. Recharge Driver Module

external switch from values of 0, 20, 40, 60, 100, and 200 μsec. In the limit, of course, the holdoff interval cannot be longer than the time between pulses and, as a practical matter, capacitor recharge occupies about a third of the interval; the holdoff maximum is therefore limited to about two thirds of the interpulse time gap.

The trigger and main power module schematics are presented in Figures 15 and 16. They both provide pulses to the same lamp module which comprises a coupling transformer and diodes to prevent damage to the power module circuit. Both power circuits are contained in the same chassis enclosure and are connected to the control unit through separate cables. Attempts to combine connecting wires within the same multiconductor shielded cable caused problems similar to those encountered when the driver circuits were positioned close to the logic elements, namely erratic behavior and breakdown at high voltages. Recharge voltages up to 270V can be accommodated by the configuration depicted and external switches allow selection of main capacitor values of 0.1 and 0.03 μF and trigger capacitances of 0.045 or 0.033 μF.

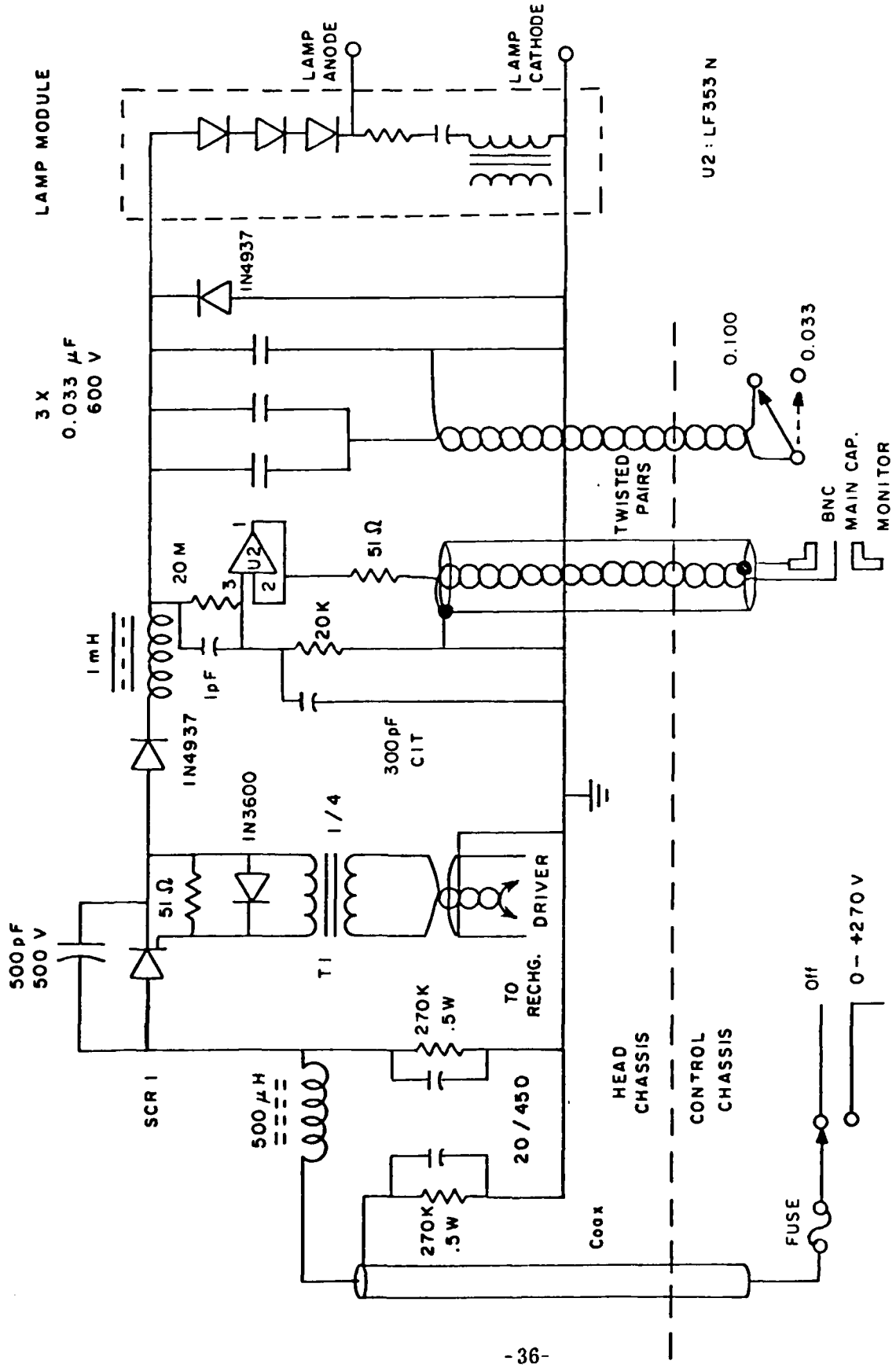

Figure 15. Lamp Main Power Module Schematic

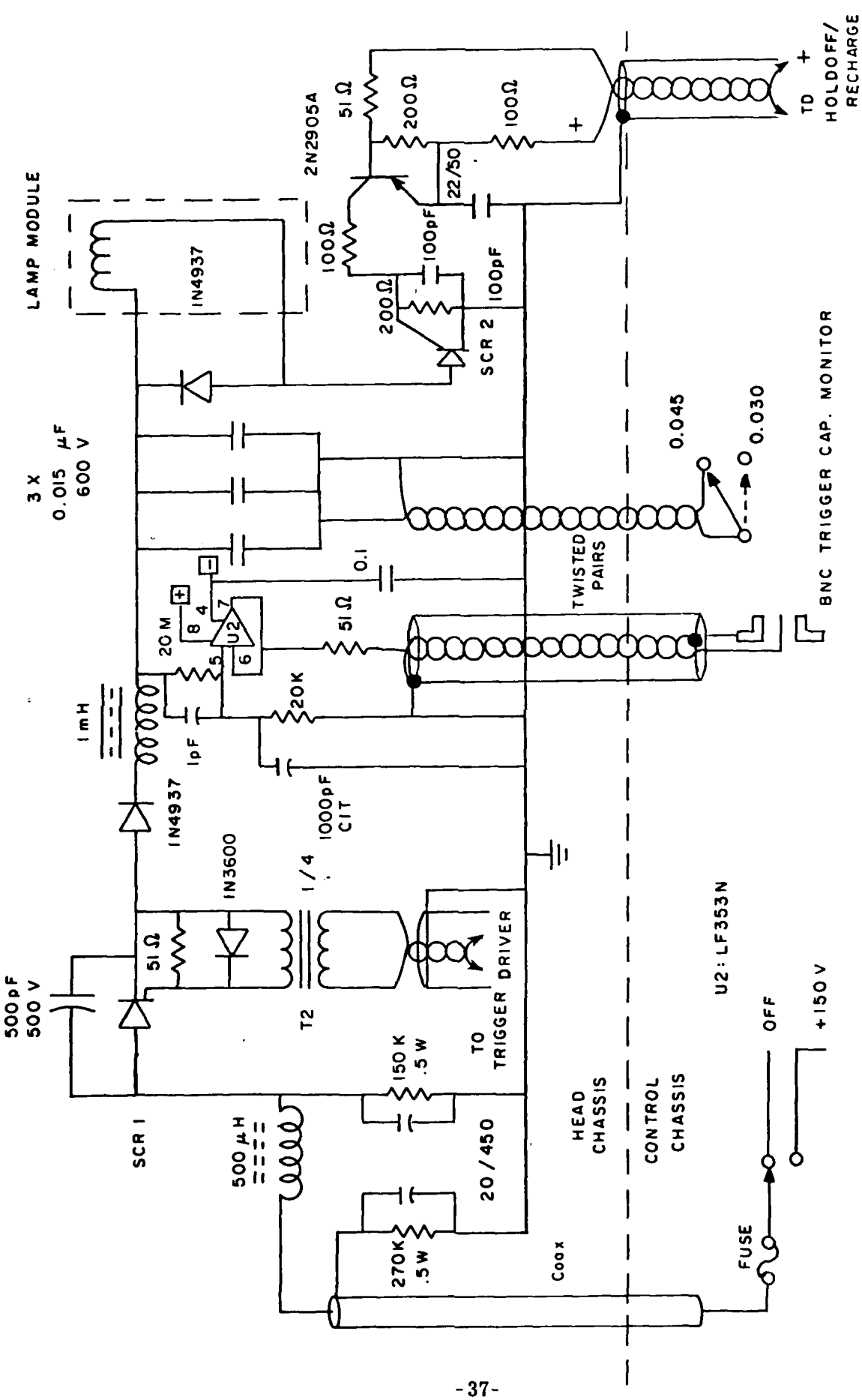

Figure 16. Lamp Trigger Power Module Schematic

4. RESULTS

4.1 Discharge Lamp Spectral Properties

The first spectral studies were performed on the 4 state-of-the-art discharge lamps built by USSI especially for the experimental program described in Ref. 8. Scans were made from 200 - 300 nm at a discharge frequency of 5 kHz and a total energy input of about 10 watts. The discharge voltage was 150 V. The four resultant spectra, a sample of which is given in Figure 17 are essentially indistinguishable from one another. The spectra appear to comprise a large number of strong atomic and ionic Xe lines superimposed on a weak continuum or very closely spaced weaker lines. The most abundant and strongest lines can be seen to lie between 225 and 260 nm. The region of greatest interest, i.e., that between about 265 and 280 can be seen to be characterized by weaker lines and a proportionately stronger continuum.

Close examination of the spectra of the two atm. lamp provided by USSI reveals a slightly larger proportion of background continuum radiation than the so called standard lamps. Subsequent experiments in which the Xe pressure was raised to 4 atm. confirmed this effect and similar results were obtained by increasing the discharge pulse frequency and thereby the power input. A typical spectrum displaying either or both of these effects is shown in Figure 18. It should be noted that in addition to what appears to be a more intense continuum, a great many more atomic and ionic lines are also present.

Neon/H_2 filled lamps are much less intense than their Xe counterparts throughout the 200-400 nm examined region and their spectra are largely devoid of strong atomic or ionic lines. A typical spectrum is shown in Figure 19. The emission features above 290 nm are almost all attributable

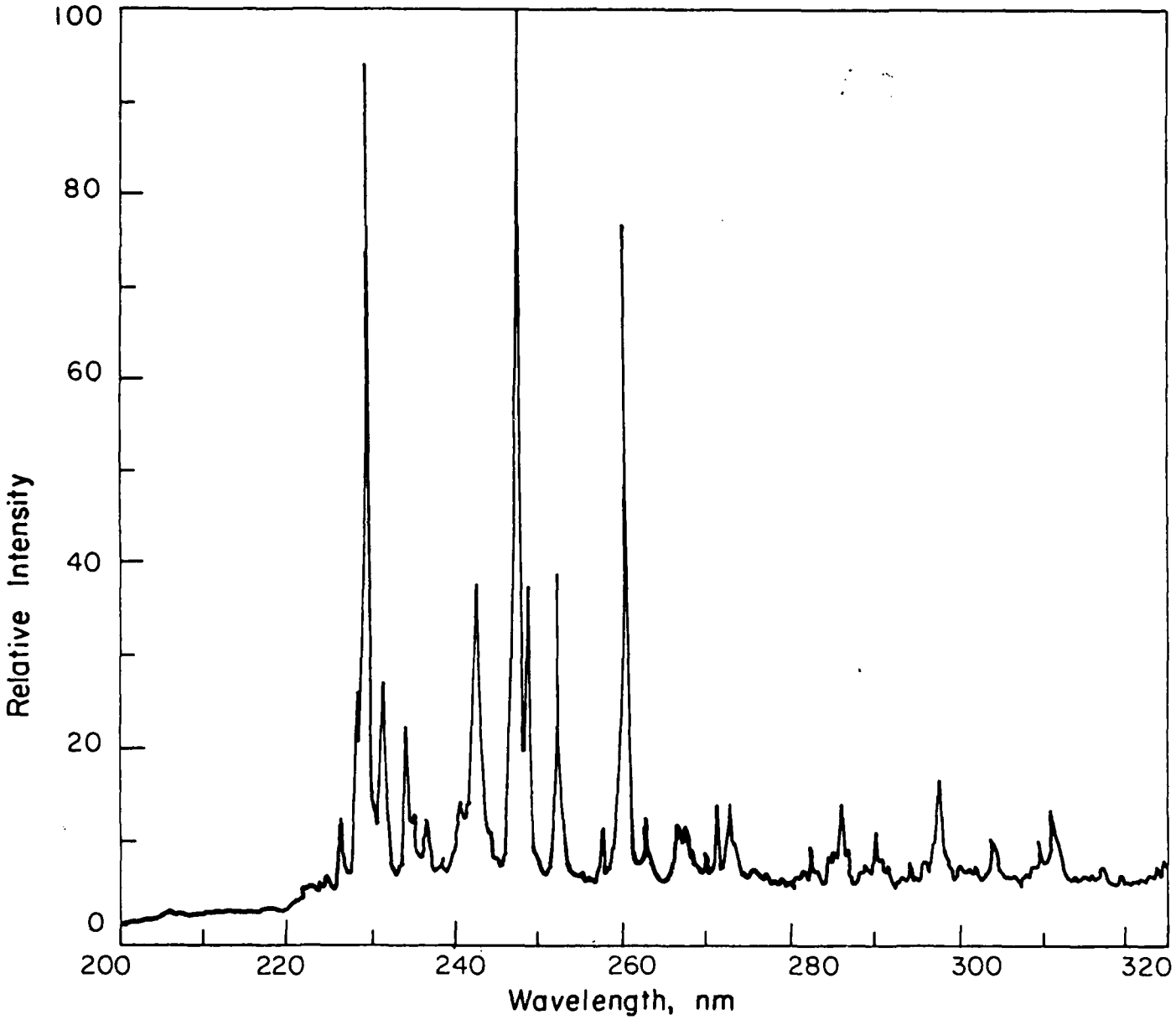

Figure 17. Spectral Output of Commercial Xe Flash Lamp

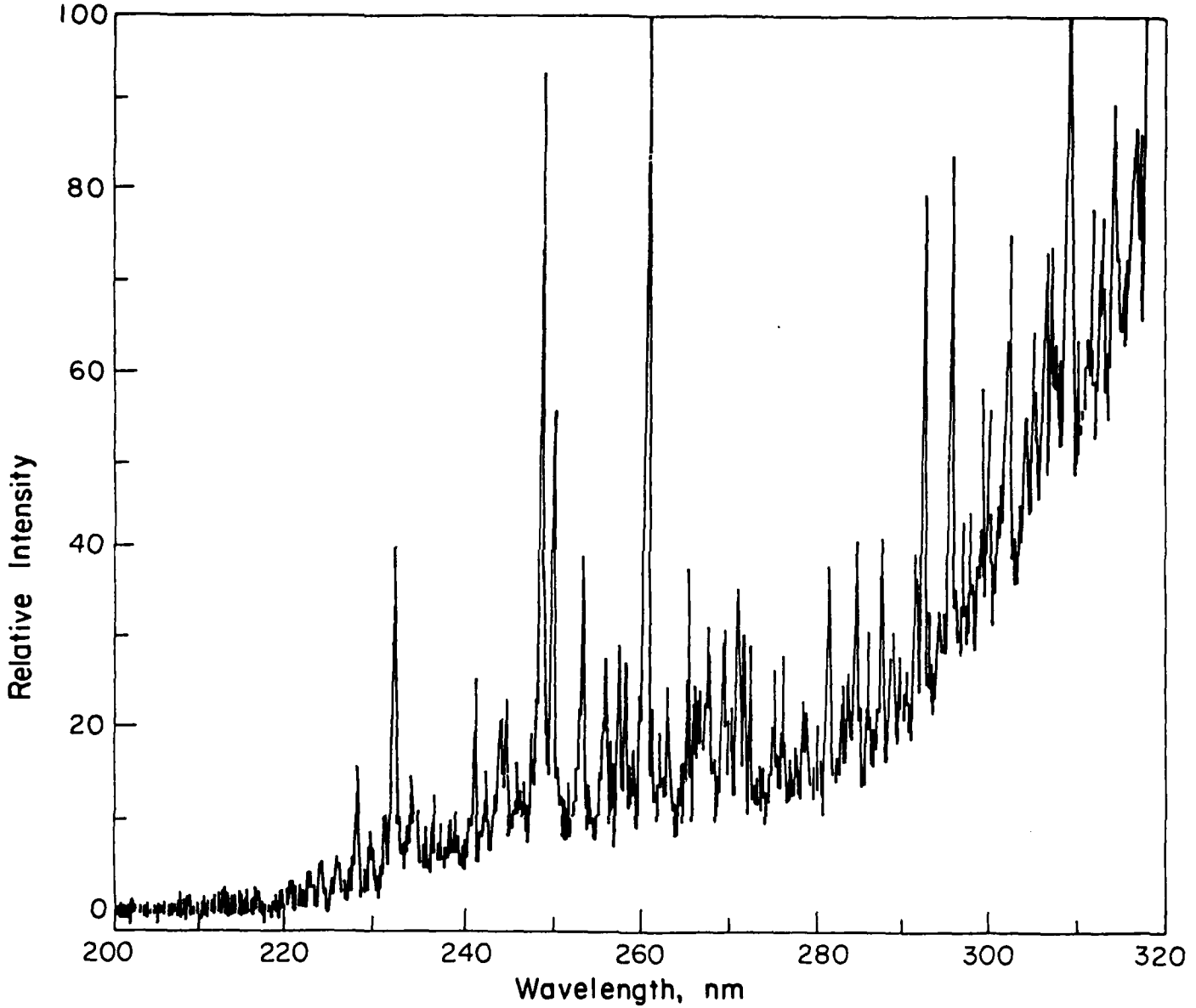

Figure 18. Spectrum of a High Pressure Xe Lamp

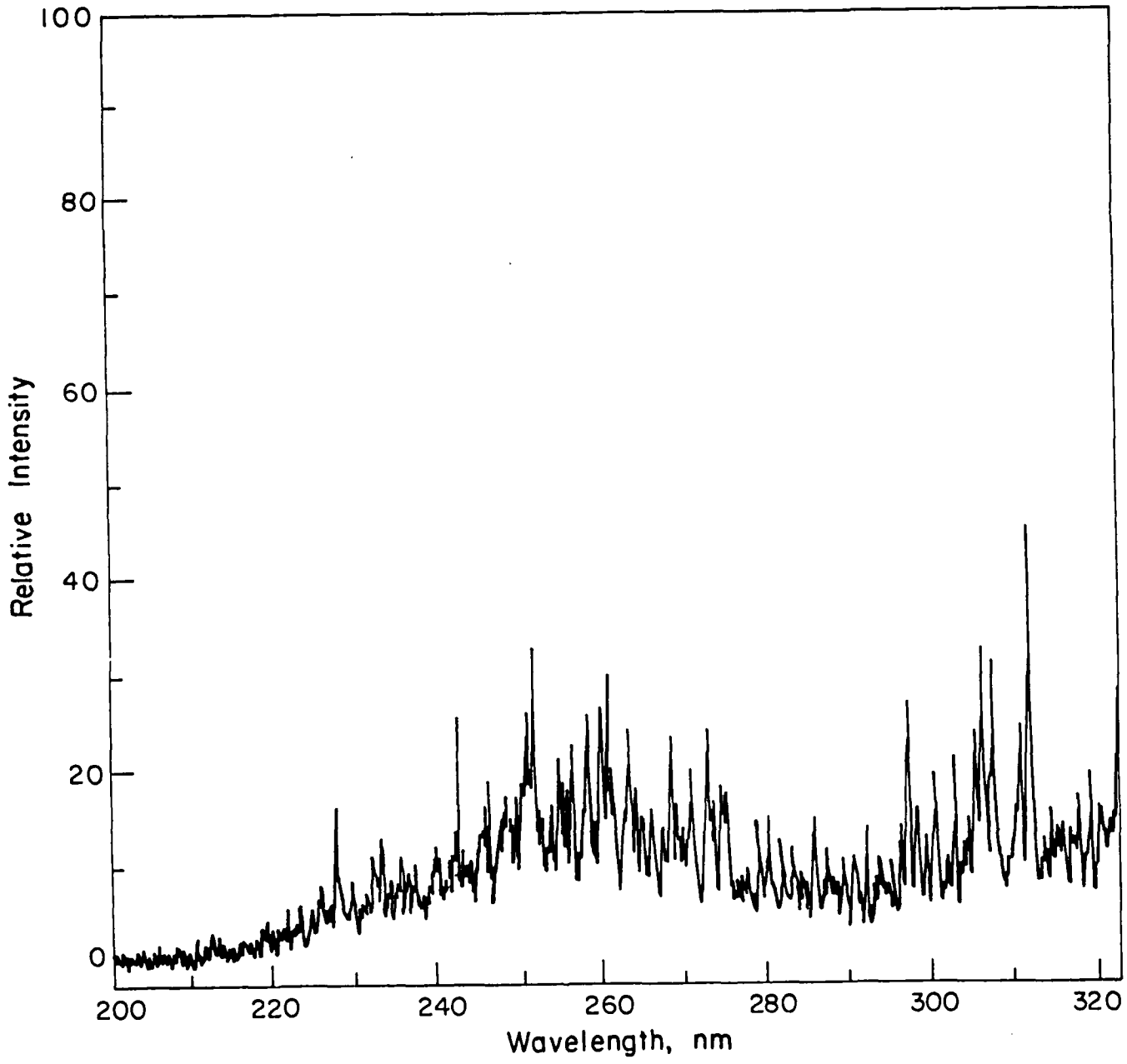

Figure 19. Spectrum of an Ne-Filled Flash Lamp

to neutral Ne(I), those in the vicinity of 270 nm are due to Ne^{+}(II) and those below about 260 nm are due to Ne^{++}(III). The intensity scale in this figure is not directly comparable to those in Figures 11 and 12; the overall intensity levels here are considerably lower. The pressure and frequency parametric behavior noted in Xe/H_2 lamps were qualitatively reproducible in these Ne discharges. The continuum radiation becomes stronger and the wavelength distribution of higher intensities is shifted toward the red.

Helium/H_2 and Ar/H_2 discharges are also much less intense in the UV than Xe/H_2 discharges. Atomic and ionic line strengths are weak compared to the continuum radiation and the continua are similar in behavior to those observed with Ne/H_2 mixtures. The He lamps at low power are noteworthy in that the spectra are dominated by emission from contaminants. Figure 20 illustrates the nature of the emission from such a low power He discharge. Helium lines are readily identifiable at 295 and 319 nm and a weak continuum underlies the entire spectral region, as in the case of the other noble gas discharges. However the strong line at 248 and the group of lines above 250 nm are attributable to C-atom emission and the emission features above 350 nm are strongly reminiscent of OH emission. The predominant contaminant in even quite pure He is normally natural gas, mainly CH_4 which in an electrical discharge produces C-atom emission and, in the presence of even very small quantities of O_2 will produce the observed radiation features.

4.2 Radiometry

After conducting a number of the spectroscopic studies described above, it became apparent that the extensive parametric studies contemplated to characterize the effects on the spectral nature of the emissions of varying gas composition, mixing ratios, electrical properties, frequency, etc. would be much more expeditiously handled by observing the output of radiometers equipped with the several bandpass filters

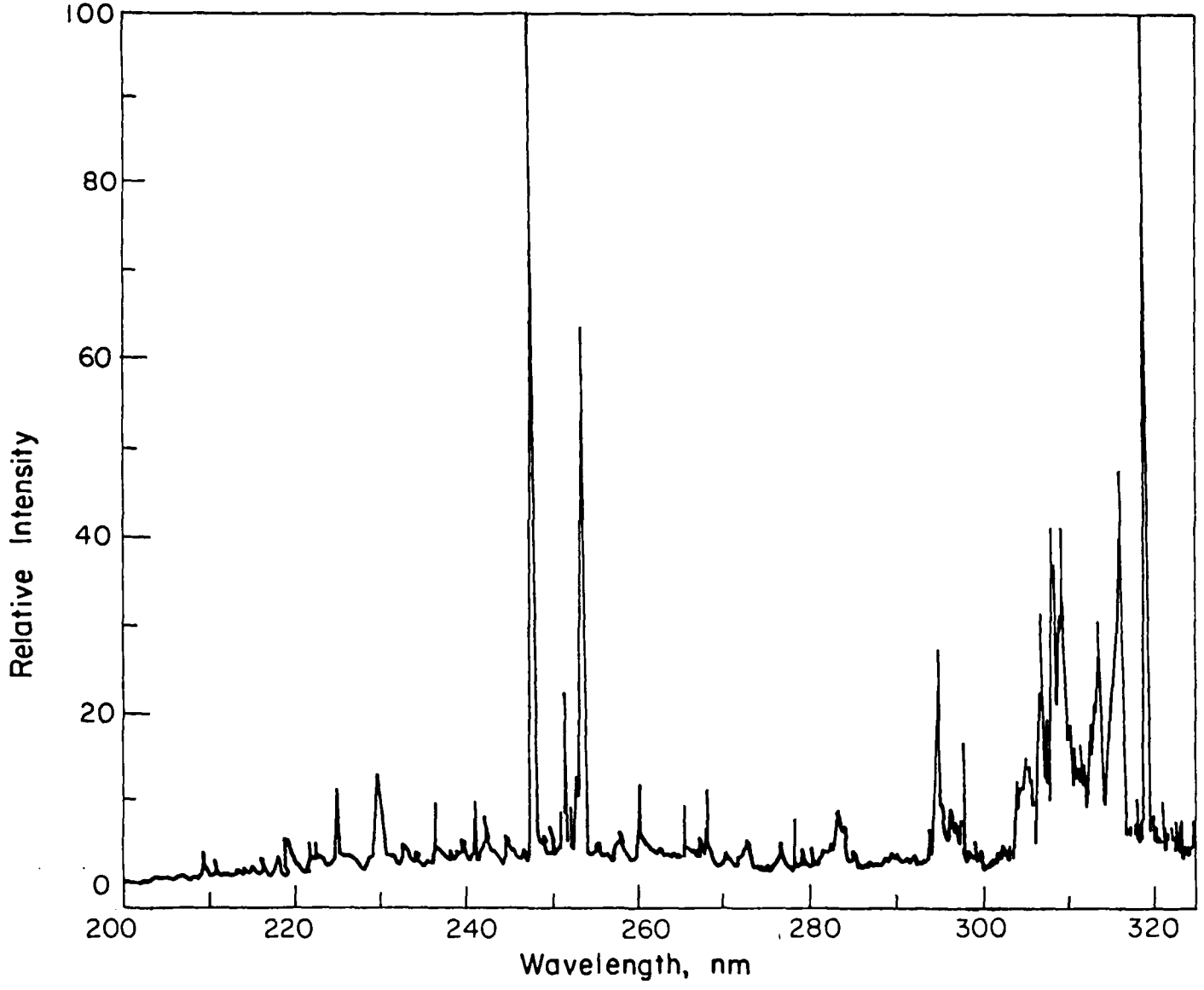

Figure 20. Spectrum of a He-Filled Flash Lamp

described in Section 2 rather than by comparing detailed spectra. Observed effects in the bandpass between 270 and 282 nm were deemed to be particularly important in view of the practical atmospheric transmission limitations which define the optimum bandpass for UV communication purposes.

A comparison of radiometer outputs at identical power input conditions for the four standard lamps prepared by USSI are displayed in Figure 21. All of this data has been corrected for filter transmission and photomultiplier response and therefore comprise direct comparisons of UV source intensities. Differences between the various bandpasses are much more readily detected here than in the spectral data of Figures 17 and 18 where the influence of contributions of narrow lines to total intensities are difficult to quantitatively evaluate by inspection. The normal pressure and higher pressure lamps can be seen to display slightly higher intensities in the bandpasses labeled A and D at opposite ends of the solar blind region than do the high H_2 and narrow gap versions of these lamps. The differences are small, however, and translate to but small increases in efficiency as reported in Ref. 8. In view of this finding that parametric variations in lamp operating characteristics appear to affect different segments of the solar blind UV to the approximately same extent and due to our priority of interest in the wavelength region 270 - 280 nm, all subsequent radiometric experiments in which various means were sought to increase lamp efficiency were conducted using a radiometer fitted with filter C (see Figure 8).

Not all lamp parameters could be varied independently of one another. the limits for the variation of each depends in some way on the set of prescribed values assigned to other parameters. Higher voltages, for example, appear to produce a much desired increase in UV intensities at the expense of intensities at higher wavelengths. However, the voltages attainable are a function of the arc gap size and the discharge pulse

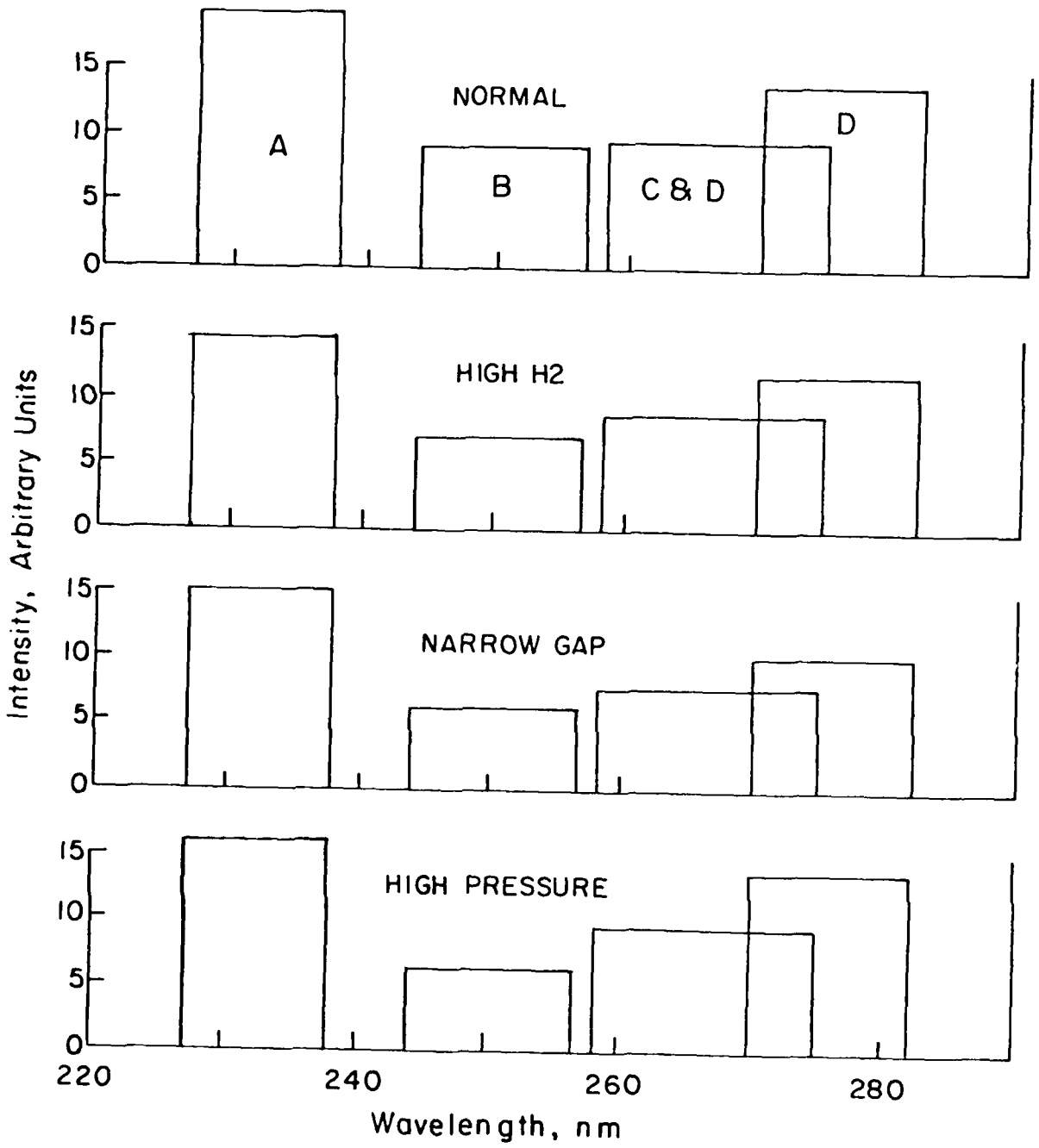

Figure 21. Radiometer Band Pass Responses to Experimental Xe Lamps

frequency. Some of the interdependencies of this complex of variables are indicated in Figure 22 in which a straightline relationship is exhibited between log I and log V^2. Unfortunately, though, there are limits to the enhancement in performance to be attained by simply turning up the voltage supplied to the lamp. As the voltage is increased, for example, in this 1.3 mm arc gap lamp configuration at a fixed discharge pulse frequency of, say, 15 kHz "holdover", or a transition from stable pulsed operation to a continuous arc occurs. In this 15 kHz case, acceptable performance is lost at fairly low voltages. Conversely, higher voltages can be sustained without holdover occurring only by employing lower pulse frequencies. In this 1.3 mm arc gap case, the lamp output in stable pulsed form maximizes at about 8 kHz. As anticipated, these performance characteristics are also a sensitive function of the arc gap size. Each spacing displays a somewhat different dependence on pulse frequency for optimum performance.

The nature of the interdependencies between discharge frequency, gap size and voltage are partially illustrated by the data of Figure 23. This data was taken using a lamp filled with the same gas mixture as that employed in Figure 22 namely, 1 atm. Xe with 0.06 Torr H_2. The I/V^2 quotient (I = intensity) can be seen to vary nearly linearily with discharge frequency indicating a nearly constant conversion efficiency of electrical to optical energy. A 0.5 mm gap width, however, can be seen to be incapable of operating at frequencies greater than about 1500 Hz without exhibiting sputtering, which creates inefficiency, and holdover, which is unacceptable operation. Increasing the gap size, in general, increases the frequency and power levels at which the lamp can be operated. However, as larger gaps and higher frequencies are reached, the conversion efficiency, i.e., the light intensity per unit power input, falls off. In the frequency range 5-10 kilohertz, the most effective gap width appears to be about 2 mm.

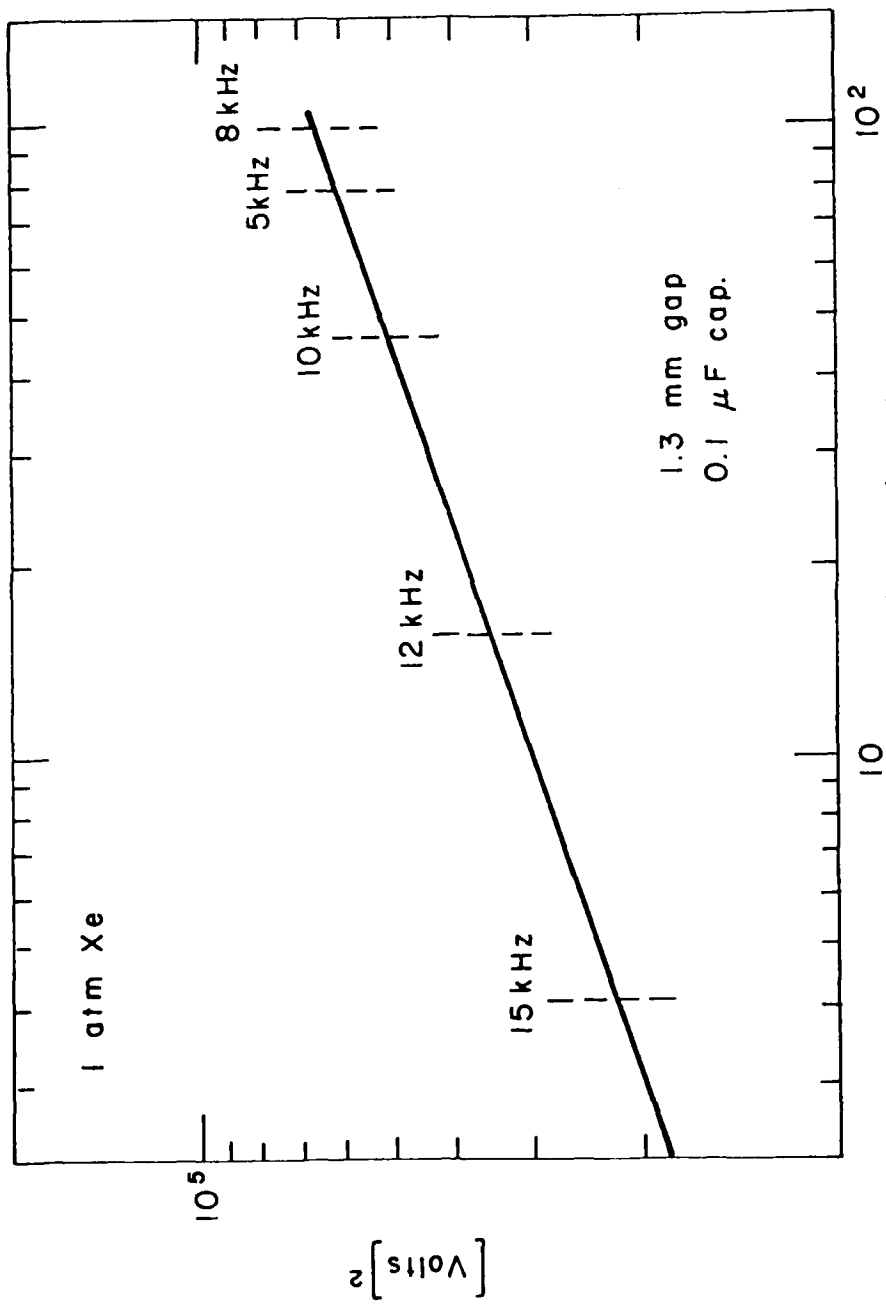

Figure 22. UV Output as a Function of Voltage for Various Discharge Frequencies. Holdover occurs above the solid line and to the left of the dashed lines for each indicated frequency.

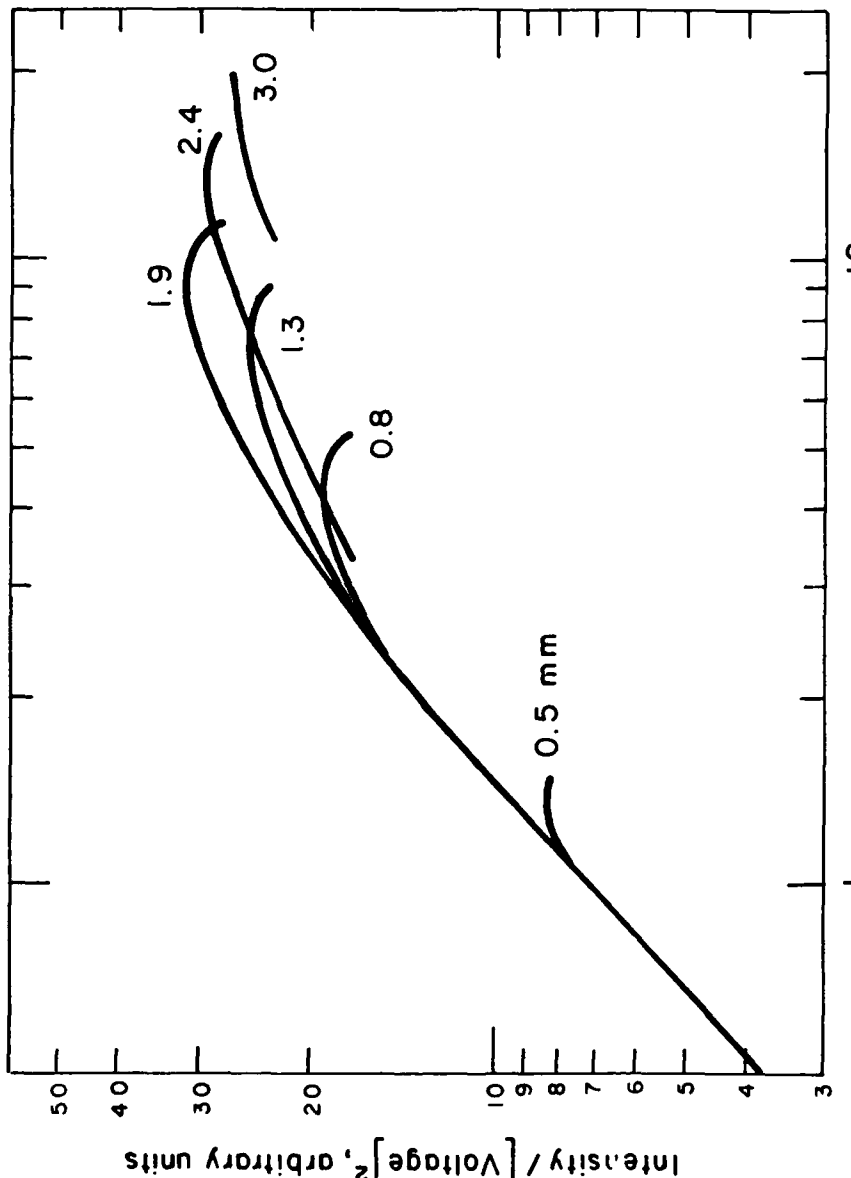

Figure 23. Effect of Frequency and Gap Size on Lamp Efficiency

Wider spark gaps require higher voltages to induce breakdown and lamps so configured can be seen to operate in a stable manner over a narrower band of frequencies with somewhat reduced light output. Lamps with large gaps appear to operate intermittently with resultant lower output levels. Figure 24 is a typical illustration of the dependence of performance on gap size. The optimum configuration for this, a lamp filled with 1 atm Xe and 0.04 Torr H_2, can be seen to lie in the interval between 2-3 mm. At smaller electrode separations, this lamp can accommodate only small amounts of input power before holdover occurs and at larger separations, as noted above, erratic behavior sets in, in which the lamp displays irregular intermittent periods of holdover and sputtering.

4.3 Gas Composition Effects

In addition to the electrical and physical configuration parameters examined, a number of experiments were conducted in which a variety of gas mixtures were formulated and tested in efforts to achieve greater UV efficiencies. As indicated by the results reported above, it was necessary in those studies to vary the lamp configuration and electrical input parameters, as well as the fill gas, since it was impossible to know, a priori, which set of parameters would be most appropriate for any given gas mixture. As noted in Section 3.1, the UV outputs from lamps in which Ne, Ar or He were substituted for Xe were considerably reduced regardless of arc gap spacing or electrical input and in spite of apparently satisfactory lamp stability. Many gas mixtures made up of these other noble gases, with or without H_2, could, in fact, be made to function satisfactorily from an operational point of view, but the lamps filled with Xe/H_2 mixtures consistently displayed higher UV efficiencies.

Figure 25 summarizes the results of a very extensive test series in which the partial pressures of both Xe and H_2 were varied over the limits practically accessible in this apparatus. Not all of the results obtained are

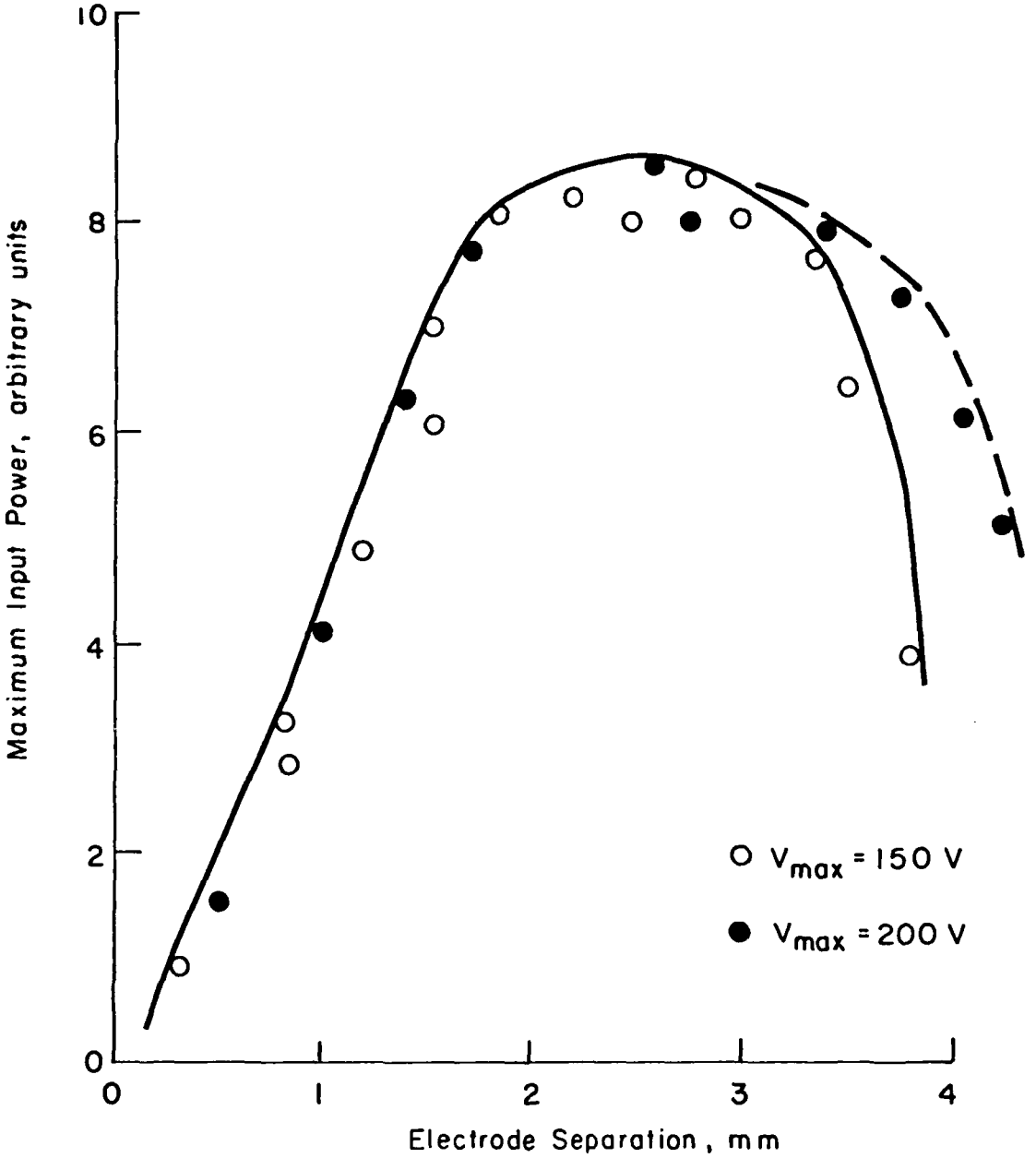

SciTec - 83-9

Figure 24. Effect of Electrode Spacing on Maximum Lamp Power Input

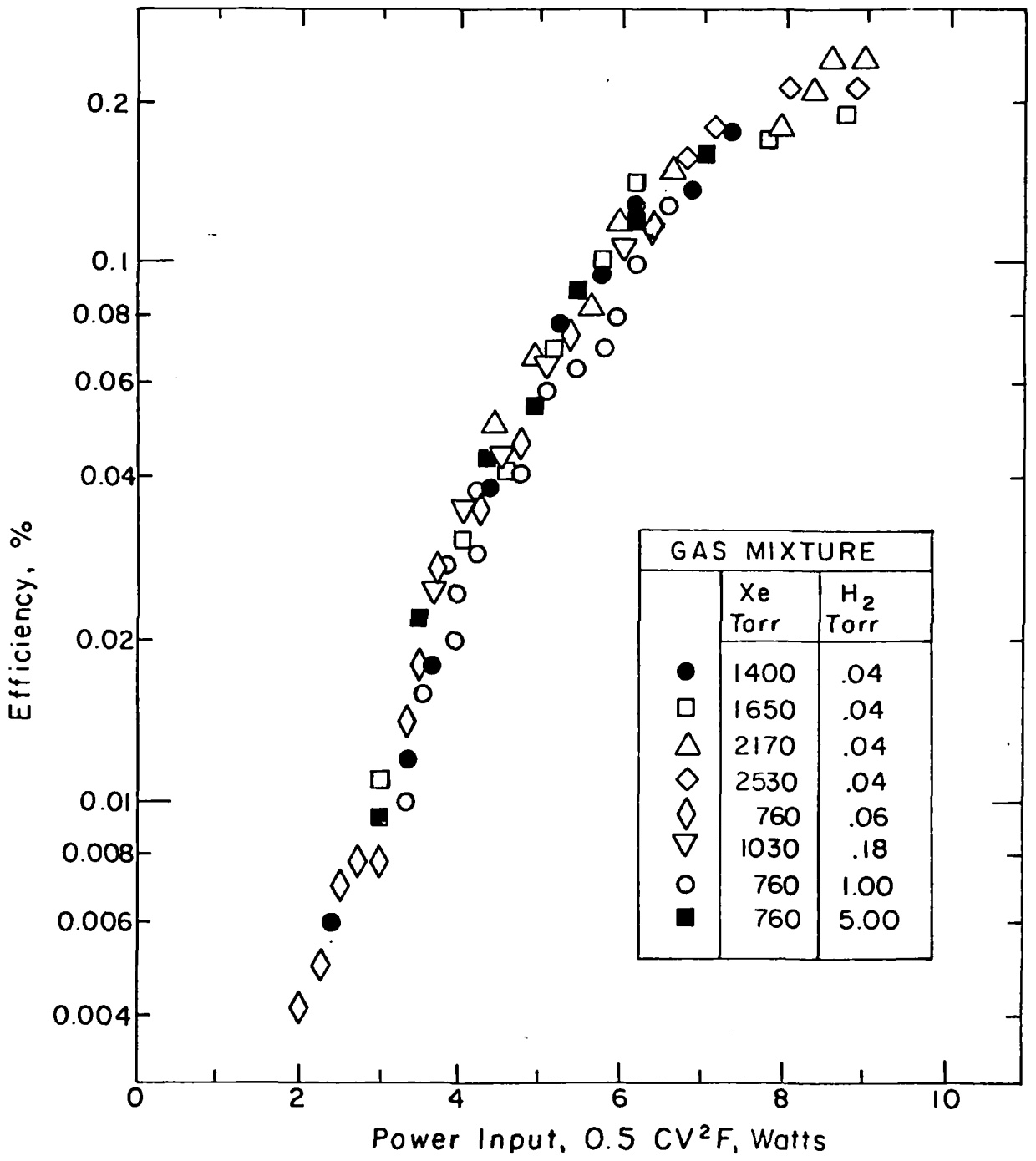

Figure 25. Lamp Efficiencies as a Function of Power Input for Various Xe/H_2 Mixtures

presented here; those from unstable discharges or less than optimum configurations are not given. The radiometer response was calibrated by directly comparing the responses to the test lamp and to the standard deuterium lamp viewed from the same distance using identical instrument settings and bandpass filters. Radiant power was then computed by integrating the output curve of Figure 9 over the appropriate bandpass interval and multiplying the result by the ratio of the observed signal strengths. Input power was taken, as indicated, as the sum of the main and trigger circuit input wattages calculated from the capacitance and the maximum recharge voltage. The lamp efficiency, ε, is thus defined as the ratio

$$\varepsilon = \frac{\text{Radiant Power Out}}{\text{Electrical Power In}} = \frac{R_x/R_d \int_{\lambda_1}^{\lambda_2} (t(\lambda)/t_{max})\, W(\lambda)\, d\lambda}{1/2\, CV^2\, f}$$

where $t(\lambda)$ and t_{max} are the filter transmissions at a given wavelength λ, and at the filter transmission maximum, respectively, $W(\lambda)$ is the deuterium lamp output power, in watts, at wavelength (Fig. 9), R_x and R_d are the radiometer responses to the test lamp and the standard lamp, respectively, C is the total capacitance in the input power circuit, V is its voltage and f is the discharge frequency.

The UV output efficiency can be seen to rise rapidly with increasing power, at least at low power input levels. Up to about 4W input, the data closely follow exponential behavior in accord with the simple expression

$$\varepsilon = 5.4 \times 10^{-6} \exp\,(0.5\, cv^2 f)$$

At higher power input levels, the gain in efficiency drops until at the highest power levels attained, about 10W, it appears that a maximum has nearly been reached or at about 0.25%.

The optimum lamp contents, i.e., the mixtures which could accommodate the highest levels of input power without the occurrence of holdover or erratic performance comprised high pressures of Xe with some small amount of H_2. At high Xe pressures, performance was not especially sensitive to the amount of H_2 present; lamps with several other H_2 partial pressures ranging from 0.04 to about 0.3 Torr were tested at an Xe pressure of 2530 Torr, for example, but the results were nearly identical to those given for 0.04 Torr. Large H_2 partial pressures do not appear to enhance lamp performance; the H_2 pressure in a lamp filled with 1 atm Xe was varied from 0.04 to 5.0 Torr with almost no change in efficiency or operating characteristics. As noted previously, high Xe pressures do enable lamps to be operated at higher power and with somewhat improved UV output. The degree of improvement realized diminishes, however, as the pressure and power input are increased. At the highest powers tested, the changes produced by variations in pressure or power were small. On the basis of this data, it would appear that the maximum efficiency attainable is approximately 0.3%. This correlates regrettably well with the observations of Ref. 8 in which power levels nearly twice as high as those employed here were found to produce efficiencies just slightly lower than the highest of those shown in Figure 25.

5. CONCLUSIONS

Although a great deal of information on the characteristics of pulse discharges and UV lamp operating characteristics were obtained in this program, the primary conclusions in terms of stated objectives must be characterized as negative in nature. No novel gas mixtures or electronic methodology was found which had any significant salutory effect on the solar blind UV output efficiency of these lamps. Some modest improvements were achieved in the operation of Xe filled flashlamps and some inherent limitations in their performance characteristics were defined. Output efficiency in the 260 - 280 nm range of prime interest was found to increase with increasing input power and voltage. The degree of improvement, however, diminishes as the power level or voltage is raised and the efficiency appears to asymptotically approach a limiting value on the order of about 0.4 percent. Conventional lamp designs need only small changes to accommodate this sort of performance improvement. Specifically, gap size must be adjusted slightly to accommodate desired combinations of frequency, voltage and power. The limits on input power are the physical strength of the lamp itself which is mainly a function of envelope thickness and the tendency of the lamp to holdover and become a continuous arc. Thicker envelopes decrease light output by virtue of a diminution in transmission. The tradeoff between transmission and efficiency factors is a fairly straightforward engineering problem. Holdover, on the other hand, can be minimized by electronic means but represents an unavoidable limit for a lamp of any configuration.

The optimum fill gas for these lamps remains Xe with small amounts of co-added H_2. Higher fill pressures produce somewhat higher efficiencies, probably by simply increasing the density of emitters in the interelectrode arc channel. Practical considerations of lamp strength and electrode seal

directly analogous to that which limits input power. However, the gain in output efficiency attainable by increasing lamp fill pressure does not appear to be as great as that derivable from raising the power input. Lamps containing two, three and four atm. of fill gas displayed only small differences in output efficiency.

6. REFERENCES

1. Neer, M.E. and Schlupf, J.M., "The Development and Testingh of an Ultraviolet Voice Communication System", Final Report Contract No. N66001-75-C-0180, A.R.A.P. Report No. 394, July 1979.

2. Compiled from Data Sheet No. F1005D-1, E.G.&G. Electro Optics Division, Salem, MA, April 1973 and from Oriel Corporation, 1979 Catalog, Oriel Corporation, Stanford, CO, pp. D7 and D22.

3. Ott, W.R. and Wiese, W.L., Opt. Eng. 12 86 (1973).

4. Data Sheet F1002C-2, E.G.&G. Electro Optics Division, Salem, MA.

5. Corliss, C.H. and Bozman, W.R., NBS Monograph No. 53, 1962.

6. Mackey, Pollack, Applied Optics 2 542 (1963).

7. Herzberg, G., Spectra of Diatomic Molecules, D. Van Nostrand, NY, 1950, p. 530.

8. Neer, M.E. and Schlupf, J.M., "Ultraviolet Transceiver Component Improvements", Final Report NOSC Contract N66001-80-C-0166, SciTec Report No. TR-81-003, February 1981.

9. Striganov, A.R. and Sventitskii, N.S., Tables of Spectral Lines of Neutral and Ionized Atoms, IFI Plenum Inc., New York, 1968.

10. Handbook of Chemistry and Physics, The Chemical Rubber Co., 38th Edition, 1956-57.

END

FILMED

7-84

DTIC